AN ABSTRACT OF THE THESIS OF

Zhengjian Yang for the degree of Master of Science in Environmental Engineering presented on February 16, 2022.

Title: Ultrafiltration Membrane Fouling in Side-stream Aerobic Granular Sludge Membrane Bioreactor

Abstract approved: _____

Xue Jin

The integration of low-pressure membrane filtration and aerobic granular sludge (AGS) reactor leads to a novel environmental biotechnological process with strong potential to overcome membrane fouling and demonstrate excellent wastewater treatment performance. However, membrane fouling mechanisms in the AGS based membrane bioreactor (MBR) are lack of systematic elaboration. In the present work, a bench-scale AGS reactor was operated for over seven months in order to investigate the effects of granule evolution, initial water flux and membrane material on membrane fouling behavior and reversibility. After 143 days of operation, complete granulation was successfully achieved in the AGS reactor which showed 97.6±1.7 % organic degradation, 94.3±2.0% NH_3-N removal, 90.6±0.8% total nitrogen removal and 98.9±1.0% PO_4^{3-}-P removal. The remarkable AGS effluent quality led to a reduction in the fouling layer formation compared to the filtration occurred before complete granulation. The combined cake-complete model demonstrated that dominant fouling mechanism is cake layer formation. The polyethersulfone (PES) membrane exhibited a better antifouling performance compared to the polyvinylidene fluoride (PVDF) membrane regardless of the AGS effluent composition. The experimental data suggest the existence of a threshold flux for fouling reversibility when PES membrane is applied to treat the AGS effluent. The combination of

physical cleaning and operating under the threshold flux can effectively control the fouling degree in side-stream aerobic granular sludge membrane bioreactor (AGSM). This, in turn, can reduce the operating cost caused from chemical cleaning and membrane replacement. Overall, the findings of this study provide comprehensive insights into the membrane fouling mechanisms and control strategy in a side-stream AGSM that will contribute towards its large-scale application in wastewater treatment.

Ultrafiltration Membrane Fouling in Side-stream Aerobic Granular Sludge Membrane Bioreactor

by
Zhengjian Yang

A THESIS

submitted to

Oregon State University

in partial fulfillment of
the requirements for the
degree of

Master of Science
Environmental Engineering

Presented February 16, 2022
Commencement June 2022

Master of Science thesis of Zhengjian Yang presented on February 16, 2022

APPROVED:

_____

Major Professor, representing Environmental Engineering

_____

Head of the School of Chemical, Biological, and Environmental Engineering

_____

Dean of the Graduate School

_____

Zhengjian Yang, Author

ACKNOWLEDGEMENTS

TABLE OF CONTENTS

TABLE OF CONTENTS (Continued)

LIST OF FIGURES (Continued)

LIST OF TABLES

LIST OF ABBREVIATIONS

AA	Acrylic acid
AFM	Atomic force microscopy
AGS	Aerobic granular sludge
AGSM	Aerobic granular sludge membrane bioreactor
ALE	Alginate-like exopolysaccharides
AOB	Ammonia-oxidizing bacteria
ATR-FTIR	Attenuated total reflection - Fourier transform infrared spectroscopy
b-EPS	Bound EPS
BOD	Biological oxygen demand
BSA	bovine serum albumin
CAS	Conventional activated sludge
CLSM	Confocal laser-scanning microscopy
COD	Chemical oxygen demand
CP	Concentration polarization
DEG	Diethylene glycol monocondensate
DI	Deionized
DMAC	Dimethylacetamide
DO	Dissolved oxygen
DOM	Dissolved organic matter
EBPR	Enhanced biological phosphorus removal
EPS	Extracellular polymeric substances
FTIR	Fourier-transform infrared spectroscopy
GAO	Glycogen accumulating organism
HA	humic acid

H/D	Height-diameter ratio
HEMA	2-hydroxyethyl methacrylate
HRT	Hydraulic retention time
LB-EPS	Loose-bounded EPS
MBR	Membrane bioreactor
MF	Microfiltration
MLSS	Mixed liquor suspended solids
MSCS	Melt spinning and cold stretching
MWCO	Molecular weight cut-off
NF	Nanofiltration
NIPS	Non-solvent induced phase separation
NOB	Nitrite-oxidizing bacteria
NOM	Natural organic matter
NPDES	National Pollutant Discharge Elimination System
OLR	Organic loading rate
PAO	Phosphate accumulating organism
PES	Polyethersulfone
PHA	Polyhydroxyalkanoates
PN	Protein
PS	Polysaccharides
PPCP	Pharmaceutical and personal care product
PVDF	Polyvinylidene Fluoride
PVP	Polyvinylpyrrolidone
RO	Reverse osmosis

RTIPS	Reverse thermally induced phase separation
SBR	Sequencing batch reactor
SEM	Scanning electron microscope
s-EPS	Soluble EPS
SMP	Soluble microbial products
SND	Simultaneous nitrification and denitrification
SPSF	Silyl sulfonate polysulfone
SRT	Solid retention time
SVI	Settling volume index
TB-EPS	Tight-bounded EPS
TIPS	Thermally induced phase separation
TMP	Transmembrane pressure
TN	Total nitrogen
TP	Total phosphorus
TSS	Total suspended solids
UF	Ultrafiltration
VFA	Volatile fatty acid
XDLVO	Extended Derjaguin−Landau−Verwey−Overbeek theory

LIST OF SYMBOLS

μ	Water viscosity
A_w	Permeability of fresh membrane
J	Water flux
J_0	Initial permeate flux
K_b	Complete blocking constant
K_c	Cake filtration constant
P	Hydraulic pressure
R_{irr}	Irreversible resistance
R_m	Intrinsic membrane resistance
R_r	Reversible resistance
t	Filtration time
V	Accumulative permeate volum

Chapter 1: Introduction

1.1   Background

Wastewater consists of toxic components to humans and the ecosystem. Untreated wastewater usually increases diseases such as cholera, typhoid fever or rotavirus. Over 1.7 million deaths were caused by untreated sewage in 2017 (UNESCO, 2017). Approximately 4.2 billion people still lack access to safe sanitation in 2021 (Ranjan, 2021). Therefore, wastewater treatment facilities are designed to accelerate the natural process of purifying water. A conventional wastewater treatment plant or conventional activated sludge process (CAS) consists of physical, chemical, and biological processes to remove solids, organic matter, and nutrients from wastewater. Although the CAS can reach high removal efficiencies of chemical oxygen demand (COD), biological oxygen demand (BOD), total suspended solids (TSS), and nutrients, three separate tanks in the biological processes (anoxic, anaerobic, and aerobic tank) requires large space and high maintenance costs. Compared to CAS, aerobic granular sludge (AGS) technology is an innovative biological wastewater treatment process that cultures activated sludge into compact granules to enhance the treatment performances. The AGS may decrease the plant's footprint by up to 75% while saving energy up to 50% (Nancharaiah and Sarvajith, 2019). As granules form into three layers (outer, inner, and core), the nutrients removal processes are complete in one tank. Nitrifiers locate at the outer layer, while denitrifiers survive in the inner layer. Meanwhile, phosphate accumulating organisms surround both the inner and outer layers. Thus, it is not essential to construct three tanks (aerobic, anoxic, and anaerobic) compared with CAS. Besides, a single tank requires less aeration and lower life cycle costs (e.g., operation, maintenance, and construction costs). Besides, sustainable use of the granular residue sludge is

another critical portion to make the effluent water reach the standards as reusable water. The granules or flocs contain extracellular polymeric substances (EPS), a complex mixture with protein, polysaccharides, lipids, humic, and nucleic acid. Recent studies indicated that EPS consisted of valuable components such as alginate-like exopolysaccharides (ALE). ALE as a polymer or gel liquid could be utilized as dye remover, soil enhancer, and flame resistance material (Van Der Roest et al., 2015; Solon et al., 2019). ALE may be extracted from the AGS using current technology with 20% of the dry sludge weight of the sludge (Cydzik-Kwiatkowska, 2021). Moreover, ALE production from EPS exceeded 2.5 times the global production from edible brown algae. This was due to the limitation of brown algae (Kehrein et al., 2020).

In the early 21st century, membrane bioreactor (MBR) has been integrated with conventional wastewater treatment processes to fulfill resource recovery, higher rejection, and reuse water production. Typical commercial MBR categorize membrane based on the pore size, including Microfiltration (MF), ultrafiltration (UF), nanofiltration (NF) and reverse osmosis (RO), ranges from 0.0001 to 10µm. MF membranes are capable of removing suspended solids, viruses, and bacteria. UF membranes are to separate colloids and proteins. NF is essentially a lower-pressure of RO, which may reject divalent ions and dissolved organics but is permeable to monovalent ions. RO can effectively eliminate all the salts and produce high-quality reuse water (Gao et al.,2011). However, the conventional MBR system's drawback is severe membrane fouling as cake layer formation or pore blocking. In this case, the integration of AGS and MBR optimizes the advantages of each system. For instance, the AGS provides a higher capacity for nitrification and denitrification than conventional MBR. Meanwhile, the integration enhances the membrane permeability and membrane cleaning efficiency by 50% and 10%, respectively,

comparing with conventional MBR due to fewer foulants established by the granules than activated sludge (Meng et al.,2009).

1.2. Aerobic granular sludge

The AGS technology has been globally investigated in lab-scale since the early stage of this century, which has been gradually applied to industrial as well as domestic wastewater treatment processes since 2011 (Tay et al.,2002; Pronk et al.,2015). The granulation, culturing activated sludge into the granules, is the core of successful biological treatment. The whole granulation process includes cell-cell adhesion, micro-aggregate formation, EPS synthesis, and maturation, which takes 30 to 60 days (Sarma et al.,2017). Each granule consists of an outer layer as the aerobic zone, an inner layer as the anoxic and anaerobic zone, and the core layer with dead cells, respectively (Figure 1.1). Some crucial elements of granules formation include hydrodynamic shear force (e.g., aeration and water flow), settling velocity or settling volume index (SVI), the composition of the substrate and organic loading rate (OLR), and reactor operation (e.g., hydraulic retention time, settling period, and sequencing batch mode), respectively (Oh., 2007; Show et al., 2012). The high shear force is primarily generated by a high aeration rate, promoting bacterial strains to establish tremendous EPS for integrating compact granular structures (Liu and Tay., 2002).

The AGS system has a lot of advantages comparing with CAS as mentioned in the previous section. However, AGS system faces many challenges, including relative long-term cultivation, disintegrating the granules after a long-term sequencing batch reactor (SBR) operation, and granules storage and reuse, respectively (Sarma et al.,2017; Sarma and Tay,2018).

Mechanisms:
(a) Proton translocation
(b) Surface charge neutralization
(c) Cell surface hydrophobicity
(d) Van der waals force

Mechanisms:
(a) Quorum sensing
(b) Environmental signals (e.g., nitrogen starvation)

Mechanisms:
(a) Effect of hydrodynamic forces (e.g., air and water flow)
(b) EPS synthesis
(c) Formation of ionic-bridges
(d) Selection pressure
(e) Growth of immobilized biomass

EPS

Aerobic zone
Anoxic/anaerobic zone
Core zone with dead cells

Microbial cells | Step 1: Cell-cell adhesion | Step 2: Micro-aggregate formation | Step 3: EPS synthesis | Step 4: Maturation | Mature granule

0-30 days | 30-60 days | 60-200 or more days

Figure 1.1 *The steps of aerobic granulation process (source: Sarma et al., 2017).*

1.3. Membrane fouling in membrane bioreactors

MBR has become famous by integrating with the CAS as the advanced wastewater treatment since the early stage of the 21st century. Many advantages have been mentioned over CAS, including small footprint requirement, higher effluent water quality, and less sludge product, respectively (Du et al., 2020; Guo et al.,2012). However, the biggest drawback of the MBR system is the membrane fouling issue, which requires extra maintenance. Potential membrane foulants can be classified into two types, including reversible and irreversible foulants. Reversible foulants result from cake layer deposition, which are usually washable by air or hydrodynamic scouring.

In contrast, non-washable reversible foulants, caused by pore blocking, require alternative chemical clean (Guo et al.,2012). Besides, foulants can be categorized into four groups, including particulates, inorganic salts, organic compounds, and microorganisms, respectively. The particulate foulants consist of large inorganic or organic particles/colloids

deposited on the membrane surfaces and reject the water transport due to a cake layer formation. Inorganic foulants include dissolved salts (e.g., calcium, magnesium, or iron) and coagulant residuals that precipitate onto the membrane surface. Organic foulants consist of various polysaccharides, proteins, humic and fulvic acids. Microorganisms also result in membrane fouling due to the attachment of bacteria with membrane surfaces; thus, biofilm form on the surface (Guo et al.,2012).

1.4. Research objectives

This research aims to develop a novel aerobic granular sludge bioreactor by integrating it with a side-stream ultrafiltration membrane for advanced municipal wastewater treatment. Moreover, this study has involved evaluating complicated relationship between EPS chemical compounds with membrane surface properties as well as fouling mechanism. To achieve these goals, specific objectives of this research consist of:

(1) systematically investigates the effect of membrane material, initial permeate flux (applied pressure), and EPS composition on the membrane fouling behavior and reversibility.

(2) obtain a deep understanding of the mechanisms governing UF membrane filtration performance during the granulation of the floccular sludge into mature granules.

Chapter 2: Literature Review

2.1 Aerobic granular sludge biotechnology

2.1.1 Affecting factors and the mechanisms of aerobic granulation

2.1.1.1 Substrate composition

The most common cultivation substrates of aerobic granules have been reported by using various organic carbon such as glucose, acetate, propionate, phenol, and ethanol (Liu and Tay, 2002; Show et al.,2012; Beun et al.,2002). The stable granulation occurred either aerobically or anaerobically. The readily biodegradable COD is absorbed in the granules under anaerobic conditions, while the substrate is converted by slow-growing bacteria in the aerobic period. Pronk et al. (2015) claimed that acetate as the easily biodegradable substrate was consumed by phosphate accumulating organisms (PAOs) or glycogen accumulating organisms (GAOs) and slowly grew into the storage polymers, which were beneficial to phosphorous removals. He et al. (2020) also concluded that acetate -fed AGS was more conducive to inhibit GAOs, which improved the stability of granule structure. Meanwhile, the anaerobic plug flow feeding led to biomass production throughout the granule, ensuring stability. The storage polymers could be oxidized by electron acceptors (e.g., nitrite and nitrate) in the inner layer, while nitrification took place in the outer layer. Besides, the adsorption substrate such as alcohols (e.g., methanol, ethanol, or phenol) did not exist in the bulk liquid, but growth still occurred throughout the granule. The stability of granules was not affected by alcohols, although they did not induce the granulation process. The acetate-fed aerobic granules were characterized as compact structures due to the abundance of rod-shaped bacteria. In contrast, glucose as the carbon source would be more likely to enhance the growth of filamentous bacteria, which led to the loose structure of the aerobic granules (Franca et al.,2018). Yuan et al. (2019) applied acetate in one AGS reactor

while glucose in another reactor to compare the nutrients removal efficiency and granules formation. At the end of the experiment on the 102nd day, the average granule size was 2 mm with a compact structure in the acetate-fed reactor. They indicated that glucose accelerated the growth of fast-growing bacteria, which reduced food-to-microorganisms (F/M) ratio. Therefore, the nutrient removal efficiency was reduced under this condition. Besides, Rollemberg et al. (2019) also concluded that acetate as the carbon source reached the highest nutrient removal rate than ethanol and glucose. The total nitrogen removal rate decreased from 72% to 44%, while total phosphorus reduced from 42% to 21% by switching acetate to ethanol and glucose. Moreover, a high concentration of glucose might increase the concentration of Polysaccharides (PS) content, which destroyed the structure of the granules (He et al.,2018). These researchers adjusted the ratio of acetate/glucose while feeding the carbon source into three systems, which were 3:1, 1:1, and 1:3, respectively. Finally, the system experienced the highest nutrient removal rate by applying the ratio of 3:1.

Overall, acetate was more supportive of forming the compact granules in the AGS reactor than other organic carbon sources, as suggested in most of the literatures above.

2.1.1.2 Organic loading rate

A wide range of organic loading rate (OLR) from 2.5 to 15kg COD/(m^3.day) supported the aggregation of mature granules (Oh, 2007). The higher OLR could accelerate the granulation (Franca et al.,2018). However, the granules could be deteriorated over the specific OLR. Recent research discovered that stable granules were maintained during the first 65 days with OLR at 15 kg COD /(m^3·day). On the contrary, an increase in OLR at 18 kg COD/(m^3·day) forced the granules to start disintegrating (Long et al.,2015). The granules instability was due to the size increase and the consequent mass transfer limitations. On the other hand, Tay et al. (2004)

analyzed the effects of OLR on the formation of granules in four sequence batch reactors. OLR was managed at 1, 2, 4, and 8 kg COD/(m^3·day) for each reactor with a 6-hr hydraulic retention time (HRT). Aerobic granules failed to appear in the reactors by utilizing low OLR at 1 and 2kg COD/(m^3·day). However, granules started forming under 4 and 8kg COD/(m^3·day) conditions on the 14th and 18th day, respectively. Only mid-range OLR, in this case, stabilized and kept granules in the system. In contrast, all the granules were eventually washed out of the system with the highest OLR condition. Tay and Liu in 2015 achieved a long-term operation (177days) in their 2L lab-scale reactor. They reduced the OLR from 12 to 6 kg COD/(m^3·day) after two weeks from the start-up to maintain stable granules. Many studies presented that nitrogen was a critical component other than COD. For instance, Wei et al. (2013) evaluated the influence of the ratio of COD/N on the cultivation of aerobic granules. The experiment occurred in a pilot-scale sequence batch reactor under a 90-day operation. They controlled the COD/N ratio from 3 to 12, where influent COD concentration was from 700 to 2400 mg/L   with NH_4^+ -N concentration at 200mg/L. In their study, the average granule size was 1.2 to 2mm. Meanwhile, low nitrogen removal occurred with a COD/N ratio of 3.32 to 5.46 due to the lack of organic carbon as the electron donor, and only partial nitrification took place. Once this ratio was adjusted over 8, nitrogen removal efficiency reached 83% and finalized at 98% with a ratio of 12. Luo et al. (2014) designed two small-scale sequence batch reactors with a COD/N ratio of 4, 2, and 1, respectively. One reactor performed the test for cultivating aerobic granular sludge, while the other one worked for flocculent sludge. The granules disintegrated with the decrease of COD/N ratio during the operating of 100 days. Liu et al. (2005) gradually increased the OLR from 0.5 to 4 g COD/L*d while decreasing the HRT by feeding glucose in their AGS reactor. The matured spherical granules were formed with a diameter of 1.2 to 1.8mm on Day17.

In general, high OLR (>12 kg COD/(m³·day)) may reduce the granulation period but it is likely to disintegrate the granules after a long-term SBR operation. Alternatively, mid-range OLR (4 -8 kg COD/(m³·day)) maintained the granules in the system.

2.1.1.3 Hydrodynamic shear force

Hydrodynamic shear forces, generated by the up-flow aeration system at the bottom of the reactor, affect the shape and structure of the aerobic granules. Wilen et al. (2018) concluded that an average superficial gas velocity ranging from 0.42 cm/s to 2 cm/s should create intense shear stress to aggregate mature granular sludge. In contrast, Franca et al. (2018) reported in their literature review that superficial gas velocity at 0.55cm/s benefited the formation of the mature granules. Besides, a patent paper controlled the superficial gas velocity at 2.5cm/s, equivalent to the airflow rate at 3L/min (Tay et al.,2004). They adjusted the air velocity between 0.8cm/s to 2.5cm/s during the experiment. No granule was formed with the low air velocity at 0.8cm/s. Instead, smooth and dense granules started forming at an air velocity of 2.5cm/s due to the high shear stress. Low concentration of DO, generated by low air velocity, enhanced the filamentous bacteria growth, which resulted in aerobic granules instability (Liu, Y. and Liu, Q.S., 2006). Recently, Zhou et al. (2016) developed a novel funnel-shaped reactor that installed a funnel-shaped steel-wire screen on the top portion of the reactor. They controlled the air velocity at 0.65cm/s in this reactor and conventional reactor. The funnel-shaped internal reactor forced large granules to move along the screen during their experiment. The large granules were then entrained by upstream bubbles and moved circularly in the top portion. In this case, mature granules still formed with a low air velocity. The mechanism behind this was due to the significant velocity changes on the granules, which sharply increased the shear stress at the top of the portion.

2.1.1.4 EPS substances

The shear stress was associated with extracellular polymeric substances (EPS) (Tay et al., 2001; Oh,2007). Zhou et al. (2016) also indicated that the shear stress in their funnel-shaped internal reactor stimulated the granules contacting with b-polysaccharides out layer structures, which finally established a dense EPS matrix. Besides, aerobic granules were recognized as one of the mixed microorganisms imbedded in the EPS matrix, which were associated with two primary components of EPS, protein (PN) and polysaccharides (PS). Franca et al. (2018) believed that the hydrophobic interaction commonly generated between granules and PN, which promoted the granular formation. Most of the other research papers supported the statement that PN's dominance maintained the granules' stability. Li et al. (2008) evaluated the ratio of PN/PS in the aerobic granular sludge membrane bioreactor. They operated the reactor for 45 days, and then ended up with an average granules size of 2.1 mm, and the ratio of PN/PS was 1:0.6. Similarly, Deng et al. (2016) investigated the influence of EPS on aerobic granular sludge aggregations. The granules were formed between 31 to 35days with an average size of 1.1mm. The PN/PS ratio was 0.6, which significantly facilitated the granules' formation. The much higher PN/PS ratio, ranging from 2:1 to 16:1, occurred in the aerobic granular sludge membrane reactor (AGSM) with a 6-hr HRT (Iorhemen et al.,2019). In addition to protein and polysaccharides, the tight-bounded EPS (TB-EPS) and loose-bounded EPS (LB-EPS), indicating the EPS distributions, were other crucial parameters that affected the stability of aerobic granules. The LB-EPS was very weak, easily destroying the structure of granules. Chen et al. (2010) concluded that LB-EPS increased with the increase of COD concentration. Meanwhile, the sludge settlement ability is also correlated with EPS content. With the increase of LB-EPS,

the sludge settlement ability decreased during the experiment period. Contradictorily, enhancing amounts of TB-EPS stabilized the granular sludge.

2.1.1.4 Reactor configuration and operations

The reactor configurations, environmental conditions, and operating cycles are vital parameters for successfully cultivating the granules and achieving excellent removal efficiency. For instance, the suitable temperature for the granulation process should be carried out at room temperature (20 to 25 °C) (Adav et al.,2008). High biomass accumulation, low SVI, high COD, and ammonia removal rate (94% and 97.5%, respectively) still could be achieved at 30°C in this study (M.H. Ab Halim et al., 2016). However, the nutrient removal rate decreased when the temperature increased to 40 and 50 °C. The granules had been gradually disintegrated from 40 to 50 °C, which inhibited the bioactivities of PAOs, nitrifying and denitrifying bacteria. The optimal pH has to be controlled between 7 and 8, as indicated in many studies (Tay et al.,2002; Xin and Qin, 2019; Stes et al.,2018). Microorganisms are hard to survive under too acidic or basic conditions, which harm the nutrients and COD removals (Lashkarizadeh et al.,2016). Besides, dissolved oxygen (DO) also influences the stability of granules. The concentration of DO ranging from 3 to 4 mg/L disintegrated the granules (de Kreuk and van Loosdrecht, 2004). In contrast, a high concentration of DO (> 7 to 8mg/L) eliminate over 90% of organic matter and nitrogen (Di Bell and Torregrossa, 2013).

The discharge port was designed at the middle of the reactor, while the feed port located at the bottom of the reactor (Tay et al.,2001). During the cycle, the granules settled down below the discharge port; thus, the appropriate HRT and settling time were essential to keeping the volume exchange ratio at 50%. Tay et al. (2002) performed their AGS reactor under a 4-hr HRT (50% of liquid volume exchange ratio). In particular, they set the settling time as 30 minutes to

allow enough time for granules to settle. Meanwhile, the height-diameter ratio (H/D) promoted the maximum specific growth rate of the microorganism. A high H/D ratio led to a shorter setup time than the reactor with a low H/D ratio. However, a low H/D ratio reactor displayed higher removal efficiency and fewer biomass products than a high H/D ratio one (Awang et al.,2016).

2.1.2 Characteristics of aerobic granular sludge

2.1.2.1 Morphology and microbial structure

The aerobic granule is a sphere with an average size ranging from 0.2 to 5 mm. The stable granule is created under high aeration rate of 3 L/min with a diameter of 1 to 1.5 mm. In comparison, a larger granule with a diameter of between 3 to 5 mm is generated under intermediate aeration of 2 L/min (Show et al.,2012). The strong hydrodynamic shear force in the reactor establishes the balance between growth and abrasive (Liu and Tay, 2002; Liu et al., 2003). The most common microbial community, including *Nitrosomonas spp.* as ammonium oxidizing bacteria (70 -100 µm from the granule surface), *Bacteroides spp.* as anaerobic bacteria (800 – 900 µm from the granule surface), PAOs and GAOs have been detected in the surface or inner layer of aerobic granules via confocal laser-scanning microscopy (CLSM) (Tay et al.,2002d; Tay et al.,2002e; Jiang et al.,2003). These active microorganisms dominate the nutrient removal in wastewater treatment.

2.1.2.2 Settleability

The settling velocity of granules, which is correlated to granules size and structure, can reach up to 70 m/h. This velocity can be seven times higher than the activated sludge flocs (10 m/h) (Oh, 2007). Besides, the sludge volume index in 30 minutes (SVI_{30}) also indicates the ability of sludge to settle. The SVI_{30} of compacted spherical granules can reach as low as 50 ml/g (Qin et al., 2004). Excellent settling results typical SVI_{30} value around 30 to 60 ml/g (Giesen et

al., 2013). Although SVI$_5$ is sometimes not measured due to minimal settling of activated sludge in 5 minutes, a ratio of SVI$_5$/ SVI$_{30}$ may eventually be close to 1, which indicates the dense and compacted granules have dominated in the system over light flocs. For example, the Nereda wastewater treatment plant reported SVI$_{30}$ and SVI$_5$ eventually reached as low as 36 ml/g and 40 ml/g, respectively (Giesen et al., 2016).

2.1.2.3 Cell surface hydrophobicity

Some researchers indicated that cell hydrophobicity was a prerequisite of the aerobic granulation process, contributing to cell-to-cell aggregation (Liu et al., 2003; Y.Liu et al., 2004). More cell-to-cell aggregation occurred when bacteria became more hydrophobic (Kos B et al., 2003; Kjelleberg S et al., 1984; Del Re B et al., 2000). Besides, Y.Liu et al. (2003) proposed two more cell hydrophobic interactions, including thermodynamics interpretation and selection pressure-induced. Especially, an integrated selection pressure-based operation was desired to enhance the granulation process. The cell hydrophobicity analysis was modified based on Rosenberg et al. (1980), which was expressed as the percentage of cells adhering to the 0.25 ml hexadecane after 15 min of partitioning. The absorbance at the wavelength of 400nm via UV spectrometer was correlated to the percentage of cell hydrophobicity. Their experiment results demonstrated that cell hydrophobicity induced and strengthen cell–cell interaction, which might be a triggering force to initiate the granulation of heterotrophic and nitrifying bacteria. Moreover, the hydrophobicity of granular sludge was nearly twofold higher than that of conventional sludge.

2.1.3 Knowledge gaps of aerobic granular sludge technology

The AGS bioreactor still has a few technical difficulties:

1. It is impossible to develop a reactor with 100% mature granules (without filamentous bacteria). A system with 100% granules requires better settling ability or very low SVI (Sarma and Tay, 2018).

2. The disintegration of granules occurs after long-term operation (e.g., >200 days) due to specific issues. The mechanisms behind the breaks of granules require further investigations. It is still challenging to maintain granules with mature shapes (Show et al., 2012).

3. Third, long-startup of AGS is another challenge for real engineering applications. The formation of granules usually takes a month or even longer, leading to low efficiency of nutrient removal during the formation period.

Furthermore, the study of the mechanisms of EPS affecting the stability of granules is still in the early stage. The proper tools for isolating, quantifying, and characterizing the EPS are unidentified. Meanwhile, the microbial group of the EPS generation is unclear as well (Franca et al.,2018).

2.2 Membrane bioreactor

The full-scale MBR application has rapidly grown in the last two decades because of highlighted advantages, including a small footprint, competitive separation of HRT and SRT, and high effluent water quality. The pros and cons of the MBR system were statistically evaluated based on the capital cost, operating cost, footprint, energy efficiency, and chemical consumption from 2014 to 2016 (K.Xiao et al., 2019). Besides, performances of treating nutrients and emerging contaminants were discussed in the following studies (Pellegrin et al.,

2015; Xiao et al.,2014; Chaudhry et al., 2015; De Luca et al.,2013; Xagoraraki et al., 2014). K.

Xiao et al. (2019) indicated the capital cost of MBR as a primary process in municipal

wastewater treatment was averagely about \$600 m^3/d, while it was \$380 m^3/d for CAS process

without tertiary treatment. The capital cost was comparable to the MBR system if the CAS was

integrated with tertiary treatment. However, the footprint of MBR (0.8 m^2/m^3/d) was about half

less than CAS (1.6 m^2/m^3/d). Besides, the operating cost for MBR was between \$ 0.11 to

\$ 0.2/m^3, compared to the CAS at \$ 0.11/m^3. Meanwhile, the energy consumption of MBR with

a median of 0.6 kWh/m^3, which was slightly higher than CAS without tertiary treatment (0.2 to

0.5 kWh/m^3) but very similar to CAS with tertiary treatment. Overall, the MBR had higher

capital, operating costs, and energy consumption than CAS without tertiary treatment but

comparable to CAS with tertiary treatment. MBR had a remarkably smaller footprint than CAS.

In addition, the COD removal rate achieved more than 95% due to high biodegradation in most

of MBRs (Sun et al.,2014). Microorganisms were able to eliminate the nutrients via nitrification,

denitrification, and other processes thoroughly (Xiao et al.,2014; Pellegrin et al.,2015). The

ammonia, total nitrogen (TN), and total phosphorus (TP) removal rate were reported comparable

to CAS with tertiary treatment over 95%, 80%, and 90%, respectively (Brepols, 2011; Melin et

al., 2006; Pagotto et al., 2014; Park et al., 2015; Pellegrin et al., 2015; Shen et al., 2012). The

pathogenic bacteria and viruses' removal efficiency was detected much higher in MBR than

CAS due to four major mechanisms: virus – MLSS adhesion, rejection/inactivation of the virus

on cake layer (Chaudhry et al.,2015). Moreover, MBR could reach up to 99.9% removal rate of

microplastics, superior to the CAS, as one of the emerging contaminants that influence aquatic

ecosystems (Lares et al.,2018; Talvitie et al., 2017). However, the MBR also faces many

challenges and lacks studies to reduce the capital/operating costs, enhance the efficiency of

aeration, and promote more effective chemical cleaning agents (K. Xiao et al., 2019).

2.2.1 Classification of foulants in MBR

2.2.1.1 Particulate/colloidal foulants

The major mechanisms of particulate/colloidal fouling consist of pore-blocking (e.g.,

pore constriction, complete blocking, and intermediate blocking), cake layer formation, and

concentration polarization (CP) (Kennedy et al.,2003). Particles or colloids initially deposit on

the membrane surface, and then the cake layer accumulates due to high drag force with

increasing transmembrane pressure (TMP) or decreasing flux (Hwang and Hsueh, 2003).

Besides, the interactions between particles, including adsorption, electrostatic repulsion, and van

der Walls attraction, are significantly near the membrane wall. Lay et al. (2010) summarized that

any constituents with higher concentration could be more strongly attached on the membrane

surface due to high CP. CP indicates that the particle concentration near the membrane surface is

higher than that in the bulk solution, leading to back diffusion into the bulk. The larger the CP,

the more intense would be the fouling, because the constituents at higher concentration are able

to interact and deposit more strongly onto the membrane.

2.2.1.2 Organic foulants

Dissolved organic matter (DOM) is the ubiquitous organic compound in wastewater,

which can be classified into two major components, such as natural organic matter (NOM) and

soluble microbial products (SMP). In particular, NOM has been detected as one of the major

foulant of polymeric membranes in MBR applications (AWWA, 2005). Besides, DOM has been

reported, leading to roughly 26 -52% to membrane fouling (Tang et al.,2010). NOM consists of

high molecular weight (MW) (>30 kDa) polysaccharides, low MW proteins, humic and fulvic

substances, which contribute to irreversible membrane fouling on UF/MF flat-sheet membrane. In contrast, hydrophobic aromatic acids cause significant flux decreases, which are reversible membrane fouling (Kwon et al.,2005). Based on the MW of NOM, three fouling mechanisms of organic foulants have been identified: 1) The adsorption of NOM into the membrane pores, where results in the blockage to the water permeability; 2) Formation of a separate gel layer on the membrane surface; 3) NOM blinds with particles to produce a low permeability particle/NOM layer on the membrane surface (Lee et al.,2008).

2.2.1.3 Inorganic foulants

Two major fouling mechanisms of inorganic salt deposit on the membrane surface includes crystallization and particulate. The precipitation of ions during crystallization results in deposition on the membrane surface. In contrast, particulate deposition occurs because of the diffusion of colloidal particulates from the bulk solution to the membrane surface (Sheikholeslami, 2000). The major inorganic salts consisting of calcium, magnesium, iron, carbonate, sulfate, and silica are determined as the mineral scale. The higher salt concentration leads to a greater inorganic scaling propensity or severe colloidal fouling.

2.2.1.4 Bio-foulants

Bio-foulants occur from bacteria cells or flocs' growth and accumulation (bio-adhesion and bio-adsorption) on the membrane surface. As one of the crucial components in cells or flocs, EPS contains polysaccharides, proteins, humic substances, nucleic acids, phospholipids, and other polymeric compounds. In particular, both hydrophobic protein and hydrophilic polysaccharides heavily contribute to membrane fouling (Yigit et al.,2008; Li et al.,2012). Other than EPS, Rosenberger et al. (2005) claimed that mixed liquor suspended solids (MLSS) also influenced membrane fouling. They reported that MLSS caused most fouling with extremely

high concentration (>15 g/L), negligible impact at medium MLSS concentration (8-12 g/L), and potential less impact at low MLSS concentration (<6 g/L).

2.2.2 Membrane characteristics

2.2.2.1 Membrane preparation and material

This section introduces flat-sheet and hollow-fiber membrane preparation methods, including phase inversion method, non-solvent induced phase separation (NIPS), thermally induced phase separation (TIPS), reverse thermally induced phase separation (RTIPS), and melt spinning and cold stretching (MSCS), respectively. Based on the size of wastewater treatment facilities and membrane area, the flat sheet membrane modules are often installed in smaller to midsize plants (2.5 to 10 MGD), whereas hollow fiber membrane modules are applied in larger plants (> 10 MGD) (Buer and Cumin., 2010).

2.2.2.1.1 Flat-sheet membrane preparation

Polyethersulfone (PES) is one of the most common materials applied in the commercial flat-sheet membrane because of its relative hydrophilicity (Abdel-Karim et al., 2017). The following research utilized PES and dimethylacetamide (DMAC) as solvents during the fabrication (Rahimpour et al.,2010). Meanwhile, Polyvinylpyrrolidone (PVP) was used as the pore former. Moreover, two monomers, acrylic acid (AA) and 2-hydroxyethyl methacrylate (HEMA) enhanced the hydrophilicity. This asymmetric PES flat-sheet membrane was prepared by the phase inversion method. PES polymer was dissolved in a mixed solution of DMAC with PVP, AA, and HEMA. The mixture was mechanically stirred at 200 rpm for 8 hrs under 25°C. Then, this solution was poured on a glass plate and stored in the water bath for one day until residual solvents and additives were leached out. Finally, this membrane was dried at room temperature for another 24 hours. Other than the normal phase inversion method, RTIPS was

reported to further enhance permeability and hydrophilicity for PES flat-sheet membrane. Liu et al. (2019) mixed various concentrations (0 wt% to 4 wt%) of silyl sulfonate polysulfone (SPSF) with PES, DMAC, and diethylene glycol monocondensate (DEG) as the cast solution. The water bath was operated under 25 and 60 °C for the RTIPS method. Consequently, the highest water flux (996 LMH) and protein rejection (79.2%) occurred by using 2 wt% SPSF by RTIPS, which were much higher than 2wt% SPSF by the NIPS method (70% of protein rejection and 300LMH of water flux).

2.2.2.1.2 Hollow-fiber membrane preparation

Compared with a flat-sheet membrane, a hollow-fiber membrane is developed with a larger surface area and higher packing density, contributing to higher flux. Thus, increasing hollow-fiber membranes have been widely installed in the AGS reactor. Similarly, NIPS and TIPS were two typical membrane preparation methods indicated in this literature review (Huang et al.,2020). In addition, MSCS had more advantages over NIPS or TIPS, which did not require additives or solvents. The mechanism of MSCS conducted polymer was spun at its melting point, and then the cold-stretching procedures were performed by a mechanical force action. The optimal temperature was about 60 °C for cold stretching. Besides, phase separation was not essential in the MSCS process.

2.2.2.2 Water affinity

The sessile-drop method, which determines the angle between a water droplet and the membrane surface, is the most common contact angle measurement (Mohammad et al.,2019). If the angle is less than 30°, the membrane is extremely hydrophilic. If the angle is between 30° to 89°, the membrane is partially hydrophilic. If the angle is greater than 90°, the membrane is hydrophobic (Zuber et al., 2013). Woo et al. (2015) applied Phoenix 300, SEO, for the contact

angle measurement. The researchers used 20 µL of DI droplet on the membrane surface, and they triplicated the data points for the measurement.

2.2.2.3 Membrane surface morphology

The membrane structure can be evaluated by high-resolution microscopies, such as scanning electron microscope (SEM) and atomic force microscopy (AFM). The SEM and AFM are complementary to each other. For instance, SEM only presents 2D images, while AFM illustrates 3D images. The measuring size distribution of SEM (2 nm to >10 µm) is wider than AFM (<1 to 20 nm) (Modena et al., 2019). S.A.Deowanetal et al. (2016) studied the UF-PES (pore size at 0.04 µm) membrane surface roughness via a Multimode AFM with Nanoscope IIIa controller(Veeco, USA) along with SEM technology. The roughness values increased from 6.59 nm of unused commercial UF-PES membrane to 9.39 nm fouled membrane.

2.2.2.4 Membrane resistance

In addition to the water flux, the membrane performance can also be corresponding to the membrane resistance according to the following equation: $J=TMP/(\mu(R_m+R_r+R_{irr}))$, where J represents water flux (LMH), TMP is transmembrane pressure (psi), μ is water viscosity, R_m is intrinsic membrane resistance(1/m), R_r is reversible resistance (1/m), and R_{irr} is irreversible resistance (1/m), respectively. The intrinsic membrane resistance is determined by the water permeability of the new membrane. The flux of fouled membrane calculates the sum of intrinsic, reversible, and irreversible resistance. The flux of membrane after cleaning calculates the sum of intrinsic and irreversible resistance. Zhang and Jiang. (2019) flushed their membrane with deionized (DI) water for 10 minutes, and then they applied 0.25% of P3-ultrasil 10 (Ecolab, cleaning USA) detergent to eliminate the foulants. They calculated the percentage of cake layer resistance and pore blocking resistance occupying in the flocs or AGS systems (% = cake layer

or pore blocking resistance / total resistance). Researchers defined floc system with granule size smaller than 0.5mm, while AGS system with granule size equal or larger than 0.5mm. Their results indicated that a much higher percentage of cake layer resistance was detected in the system with flocs (71%) than AGS (46%), while higher pore blocking resistance in the AGS (54%) than flocs system (29%). The large size of AGS was difficult to deposit on the membrane surface, which was feasible to be flushed by DI water. However, EPS of AGS entered the membrane inside or accumulated, afterward blocking membrane pores.

2.2.2.5 Membrane surface charge

Surface charge characteristics and interaction energy models are common methods to analyze the chemical compositions and foulants on the membrane surfaces. For instance, zeta potential is the most straightforward way to analyze the electrostatic repulsions between colloidal particles and membrane surface. Some key parameters significantly influence the zeta potentials, including ion concentrations and types, pH, and temperature, respectively. In this study (Han et al.,2011), the researchers modified the PVDF membrane with various concentrations of chlorosulfonic acid and 1,4-dioxane (DS) to improve the hydrophilicity. Pristine and modified PVDF membranes' zeta potential was measured via electrophoretic light scattering spectrophotometer (ELS-8000, Otsuka Electronics Co., Japan). The measurement was performed at 10 mM KCl solution with pH ranging from 2 to 9. Their zeta potential results showed that zeta potential value decreased with pH increasing due to adsorption of anions (e.g., OH^- and Cl^-) as well as dissociation of sulfonic acid groups. The lowest zeta potential indicated the highest concentration of DS (2.99 wt%). Alternative to detect the electrostatic repulsion of salt ions, the zeta potential can also determine the critical foulant compounds, such as proteins and humic acid (HA). Fu et al. (2017) investigated the effects of foulants on various commercial PES

membranes. Both 200 mg/L of bovine serum albumin (BSA) and 10 mg/L of HA were simulated as the foulant compounds. The zeta potential for BSA at pH of 7.46 was -20.6 mV, while HA was -45.8 mV at pH of 6.57 on fouled PES membrane, which suggested stronger electrostatic repulsion was generated by BSA foulant.

Besides, interaction energy theory can be applied to interpret the membrane-foulant adhesion force. For instance, the extended Derjaguin−Landau−Verwey−Overbeek theory (XDLVO) evaluates the interaction energies, which is the sum of Lifshitz−van der Waals, electrostatic double-layer, and Lewis acid−base energy (Fu et al., 2017; Sun et al., 2018). Fu et al. (2017) summarized that electrostatic double-layer and Lewis acid−base were two dominators in the total energy interaction for BSA fouled membrane, while electrostatic double-layer interaction energy was a primary contributor for HA fouled membrane. However, Sun et al. (2018) claimed that Lewis acid−base interaction energy was more significant than electrostatic double-layer interaction energy in their BSA and HA mixtures.

2.2.3 Operation mode

The permeate flux indicates the water or salts passing the membrane surface under a certain period. The MBR can be operated in two modes: (1) constant flux and (2) constant pressure. The first mode is to control a constant flux by using a peristaltic pump as permeate pump. Then, the pressure gauge records the TMP variation over time. The increase of TMP indicates the increase of foulants deposited on the membrane surface. In contrast, the flux decline under the constant pressure mode implies the increased foulants on the membrane surface. These two pieces of literature conducted filtration under these two methods (Wang et al.,2018; Iorhemen et al.,2019). Wang et al. (2018) operated their AGSM under constant pressure mode.

In contrast, Iorhemen et al. (2019) controlled a constant flux at 12.5 LMH while monitoring the transmembrane increase. They cleaned the membrane by water jet until TMP raised to 50 kPa.

To compare fouling and organics rejection under constant flux with constant TMP mode, D.J. Miller et al. (2014) adjusted flux at 25, 40, 55, 85, and 100 LMH, corresponding to TMP at 2.7, 4.1, 5.3, 7.6, and 9.7 kPa, respectively. Under constant flux mode, they realized that modest increases in TMP below the threshold flux (62 LMH), while rapid increases in TMP above the threshold flux. In contrast, all constant TMP experiments displayed qualitatively similar behavior regardless of whether flux was below or above the threshold flux. By plotting the total resistance as the function of permeate volume/filtration Area, the resistance under the constant flux initially reached the same level as the constant TMP. However, it significantly increased thereafter. In contrast, the total resistance showed a concave down increase, and then it remained at a plateau under the constant TMP mode (Figure 2.1). Besides, the organic rejection results (all >97% under both modes) indicated that constant flux had slightly higher rejection rate than the constant TMP. Above the flux threshold, the rejection rate increased with the increase of TMP due to the foulant accumulations on the membrane surface. Under the constant TMP mode, the decrease of rejection with the increase of flux was due to the enhanced concentration polarization at high TMP. Their study results summarized that total membrane resistance and foulant was low for constant flux mode while high for constant TMP mode below the flux threshold. Opposite results occurred below the flux threshold.
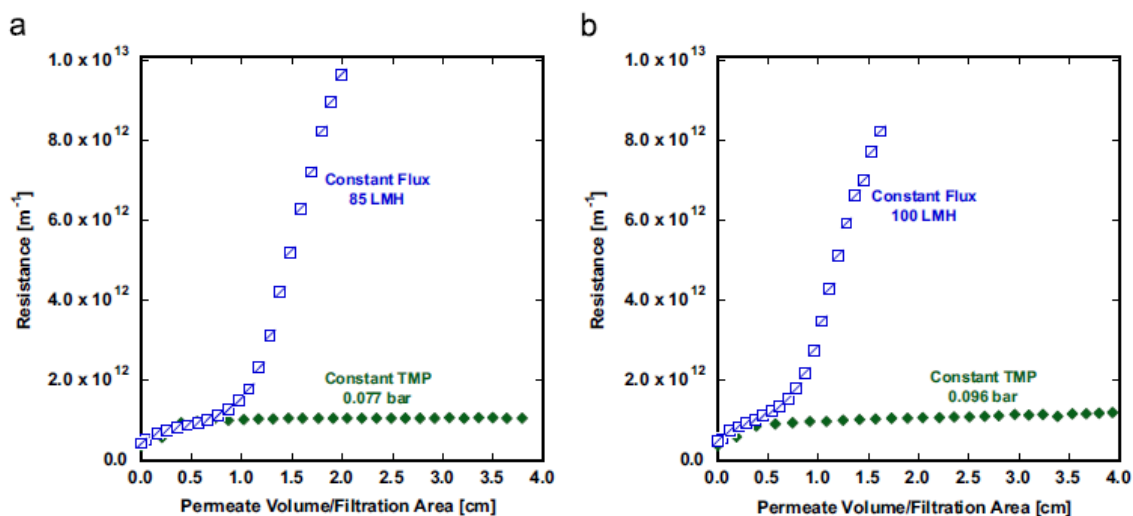
Figure 2.1 *Comparisons of resistance evolution during constant flux and constant TMP experiments at fluxes above the threshold flux at 62 LMH (source: D.J. Miller et al., 2014).*

2.3 Aerobic granular sludge membrane bioreactor (AGSM)

2.3.1 Background of AGSM

According to some previous work, the integration of AGS and MBR may reduce the potential membrane fouling (Iorhemen et al.,2016; Iorhemen et al.,2017; Zhang et al., 2021). Three major mechanisms support this phenomenon:

1. The large size and rigid structure of granules reduce membrane pore blocking and cake layer formation.

2. EPS is mostly used up in the granule formation, and thus less soluble EPS is present in the mixed liquor to accelerate membrane fouling.

3. Granules can form a positive scouring force by collision and friction with the membrane surface in the submerged AGSM.

The AGSM can be classified as side-stream and submerged configurations. The side-stream AGSM indicates that the AGS bioreactor is integrated with an external membrane module,

whereas the membrane module installed in the AGS reactor is called as submerged AGSM. The advantage of side-stream AGSM is fewer membrane foulants than submerged AGSM since only the supernatant (e.g., only soluble EPS rather than bounded EPS) is discharged for further filtration. The granules have potential to, consisting of bounded EPS, accumulate on the membrane surface in a submerged AGSM. However, the submerged AGSM requires fewer footprints than a side-stream AGSM due to its internal installation of the membrane module.

2.3.2 Performance of AGSM

2.3.2.1 Rise of TMP

Iorhemen et al. (2019) operated their submerged AGSM under a constant flux mode. The membrane was essential for an uninstalled clean when the TMP reached 50 kPa. In this case, Run1 (189 mg/l TOC and 8 hr HRT) and Run3 (104 mg/l TOC and 10 hr HRT) were the only two reached 50 kPa, while TMP of Run2 (266 mg/l TOC and 10hr HRT), Run4 (104 mg/l TOC and 6 hr HRT), and Run5 (266 mg/l TOC and 6 hr HRT) raised to 8 kPa, 42 kPa, and 6 kPa instead of 50 kPa. In this situation, both Run1 and Run3 were detected with high PN in the soluble EPS (s-EPS). On the contrary, low concentration of PN in s-EPS but a high concentration of PN in TB-EPS among Run 2, Run 4, and Run 5, respectively, suggested most EPS in the granules creating smooth filtration conditions.

2.3.2.2 Permeate flux decline

Wang et al. (2018) operated the side-stream AGSM under a constant pressure mode at 300 kPa to compare the flux decline of UF-PES membranes with various molecular weight cut-off (MWCO) at 5, 10, 20, 30 and 100 KDa and hydrophilicity. The larger contact angle (or more hydrophobicity) of UP100 (74.6 ± 1.3°) and UP020 (76.9 ± 1.8°) resulted in more significant water flux decline than other membranes at the end of the experiment. Besides, the flux decline

also was affected by the pore size. For instance, the foulant particles were more feasible to enter the pores, which caused higher pore blocking fouling. The flux decline increased with increasing of membrane pore size or MWCO (5 to 100 KDa). However, one exception occurred on UP030 (MWCO = 30 KDa) that the flux decline was lower than UP020 (MWCO = 20 KDa) and UP100 (MWCO = 100 KDa). As discussed above, UP100 and UP020 had higher contact angles than UP030 ($70.6 \pm 1.8°$), which displayed hydrophobicity as a slightly more dominated foulant issue than pore size or MWCO.

2.3.2.3 The role of EPS on membrane fouling via 3D-EEM and FTIR analysis

Iorhemen et al. (2019) witnessed a higher concentration of PN in s-EPS for Run1 and Run3 than other runs in their submerged AGSM. Moreover, Run1 and Run3 reached up to 50 kPa of TMP. Therefore, PN in the solution was correlated to the membrane fouling. Besides, much higher EPS contents (PN and PS) occurred in Run2 and Run5, corresponding to the lowest TMP, demonstrating that higher TB-EPS would cause less membrane fouling. This phenomenon was consistent with previous research that TB-EPS was independent of membrane fouling (Wang et al.,2009). Based on the statistical analysis of the effect of TOC and HRT on EPS, TOC increased while the increase of TB-EPS. HRT may affect the TB-EPS with a certain TOC (104 mg/L). For TOC at 104 mg/L, TB-EPS decreased while the HRT was increasing. However, no significant TB-EPS change happened with the increase of HRT when TOC was 266 mg/L. Besides, both s-EPS and HRT influenced the membrane fouling. PN in the EPS promoted the cake layer formation on the membrane surface due to the high stickiness (Chen et al.,2007). Meanwhile, low HRT may cause overwhelming of filamentous bacteria and high biomass concentration, which induced more pore blockage and bio-cake deposits (Meng et al., 2007; Huang et al., 20011).

In the FTIR experiment, one peak of Run1 to Run4 indicated the wavelength region for protein, while two peaks of Run5 implied not only protein in TB-EPS but also humic acid was detected, which was caused by the aging granules in Run5 (Iorhemen et al.,2019). Alternatively, Wang et al. (2018) operated FTIR to investigate the functional groups of the foulants on the PES membrane surface from their side-stream AGSM system. This fundamental study realized substances with carbon and nitrogen led to membrane foulants. Meanwhile, some irreversible foulants were caused by the alkaline cleaning agent, 0.25% of P3-ultrasil 10. The other research evaluated functional groups for AGS with various sizes (0.5 mm to 1.7 mm) (Zhang et al.,2019). Interestingly, the most severe foulants occurred at the critical size (1 to 1.2mm) of granules due to the adhesion of EPS as well as the compact structure of cake fouling layer. Granule size larger than 1.2 mm resulted in high porosity of cake layer, while granule size less than 1mm intensified the pore blocking.

In addition to FTIR, NOM, including protein, polysaccharides, humic or fulvic substances, can be detected by three-dimensional excitation-emission matrix (3D-EEM) fluorescence spectroscopy. A series of emission and excitation spectra wavelengths are collected, and then fluorescent compounds display in complex mixtures (Wang et al.,2009). The following procedures summarize the normal operation of 3D-EEM: A 1-cm quartz cuvette with four optical windows is used for the analyses. Emission scans (e.g., DI water as blank and wastewater samples) are performed from 220 to 550 nm at 5 nm steps, with excitation wavelengths from 220 to 450 nm at 5 nm intervals. The detector is set to high sensitivity, and the scanning speed is maintained at 1200 nm/min. Besides, the slit widths for excitation and emission are 5 nm and 2.5 nm, respectively. Finally, the 3D-EEM contour plots can be generated by MATLAB using matrix code. The Y-axis illustrates the excitation wavelength, while the X-axis demonstrates the

emission wavelength. The third dimension expresses the fluorescence intensity with contour lines (Liu et al.,2011). In their study, the key fluorescence peaks referred to as fluorophores C (humic-like substance) within Excitation/Emission range of 310/420, T1 (tryptophan-like protein) within Excitation/Emission range of 280/340, and T2(tyrosine-like protein) within Excitation/Emission range of 220/335, respectively. Accordingly, the intensity of each NOM was identified as C, T_1, and T_2 at 298, 283, and 536, respectively, in the raw wastewater. The peak intensities were weakened significantly after the treatment, which reached 154, 71, and 96.5 for C, T_1, and T_2, respectively. Iorhemen et al. (2019) detected protein-like substances in TB-EPS samples via 3D-EEM, corresponding to the analysis of TMP and protein concentration; thus proteins in TB-EPS are contributed to the membrane fouling in their study.

2.3.2.4 Surface roughness analysis

Wang et al. (2018) conducted the analysis of the morphology of the UF membrane surface by integrating SEM with AFM. Those white spots represented the membrane foulants illustrated by SEM images. For AFM images, the rough area (or bright area) was increased in the fouled membrane, compared with the unique ridge and valley shape (or dark area) on the virgin membrane. Only a few white spots or rough areas are distributed via the UF membrane surfaces. Therefore, they believed that pore blocking was the major foulants without a clear cake layer occurring on the membrane surfaces.
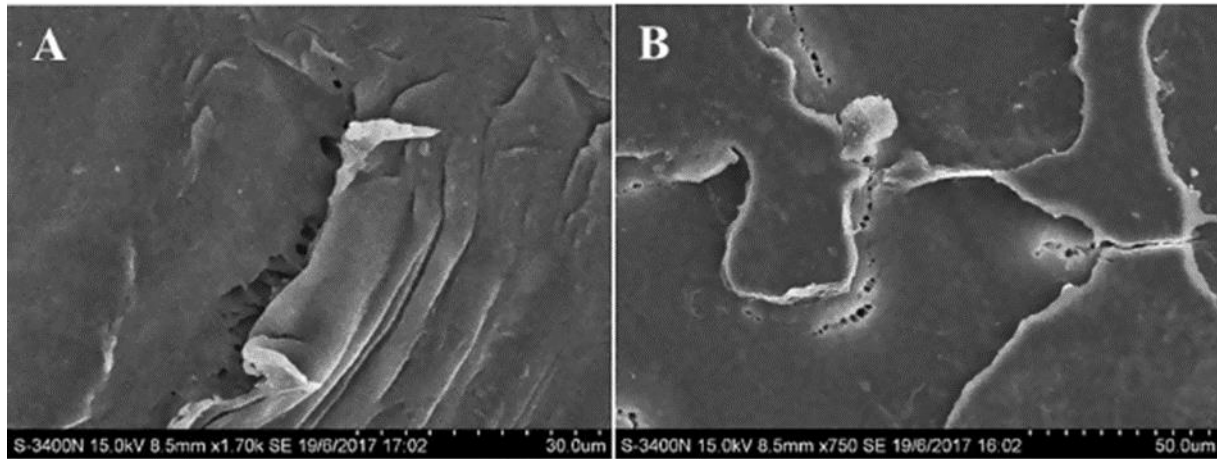
Figure 2.2 *SEM images of the pristine UF membrane (A), fouled UF membrane (B) (source: Wang et al.,2018)*
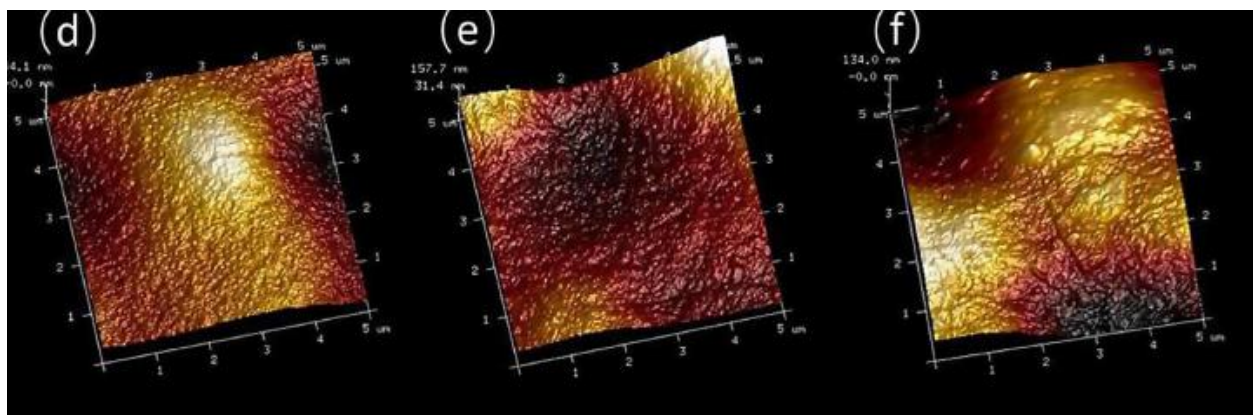
Figure 2.3 *AFM images and roughness on new (d), fouled (e), and cleaning (f) UF membranes (source: Wang et al.,2018)*

2.3.2.5 Organic and nutrients removal

The submerged AGSM system achieved 98% TOC removal, 99% ammonia removal, and 52% total nitrogen removal (Iorhemen et al.,2019). In some periods, a relatively high concentration of nitrate and low total nitrogen removal indicated a lack of denitrification occurred during these days. In addition, the side-stream AGSM reached 90.5% of COD removal, 94.84% of TN removal, and 97.07% of TP removal, respectively (Wang et al.,2018). Because

granules involved aerobic, anoxic, and anaerobic conditions based on their structure, nitrification, denitrification, and phosphorous removal took place in the same tank. Nitrification was dependent on the ammonia-oxidizing bacteria (AOB) and nitrite-oxidizing bacteria (NOB). *Nitrosomonas* and *Nitrospira* were the most populated AOB and NOB in the community. Denitrification took place under the anaerobic condition that nitrate was converted to nitrogen. *Paracoccus denitrificans* and *Pseudomonas stutzeri* were two major bacteria supporting the full denitrification. The enhanced biological phosphorus removal (EBPR) occurred in the granules. Under anaerobic conditions, phosphate accumulating organisms (PAOs) uptake volatile fatty acid (VFA) by secondary transport. The glycogen accumulating organisms (GAOs) and PAOs will compete for the available organic substrate. The dominance of GAOs in AGS is associated with a decrease in P removal. Under aerobic conditions, polyhydroxyalkanoates (PHA) are oxidized, and subsequent energy release is used for the uptake of P.

2.4 Summary

This chapter introduced fundamental concepts and knowledge gaps of AGS technology. Besides, typical membrane foulants, including particulate, inorganic, organic, and bio-foulants, were discussed based on chemical and biological characteristics. The integration of AGS and MBR systems was suggested to optimize advanced wastewater treatment performance. Early results of the integration of aerobic granular sludge and membrane filtration show remarkable membrane fouling reduction. However, the understandings of the stability of granules under long-term operation as well as the fouling mechanism of EPS on the membrane surface are still in an early stage, which requires essentially further investigation.

Chapter 3: Materials and Methods

3.1 AGS Reactor Setup and Operation

The plexiglass AGS reactor had an effective working height of 120 cm and an internal diameter of 5 cm (Figure 3.1). A high H/D ratio can establish the effective hydraulic shear forces to aggregate microbials, thus accelerating the granulation and promoting the biomass functions (Liu and Tay, 2002). Aeration was performed at the bottom, and the air up-flow velocity was controlled at 2.5 cm/s (or DO between 8 to 10 mg/L) by the air flow controller (Masterflex, Cole-Parmer, Vernon Hills, IL, US) for adequate shear force and fine air bubbles. The reactor was continuously operated in successive cycles (or HRT) of 4 hrs. Each cycle consists of 5 min influent feeding 210 min aeration, 20 min settling, and 5 min effluent withdrawal. The volumetric exchange ratio was set at 50%. This study used a fast-anaerobic feeding strategy where the influent was fed to the reactor within a few minutes without aeration through the side port close to the bottom of the reactor. This feeding method was reported to accelerate granules formation (Iorhemen and Liu, 2021). Moreover, easily biodegradable carbon was converted into storage polymers, which resulted in the fast heterotrophic growth as well as large-size granules formation (Pronk et al.,2015; Carta et al.,2001). Meanwhile, the settling phase allows denser sludge or granules to sink at the bottom of the reactor while the fluctuating sludge is drained from the middle port (effluent port) of the reactor. Return activated sludge collected from Corvallis Wastewater Treatment Plant (Benton County, OR) was used as inoculum for the start-up of the reactor. The AGS reactor was fed with the mixture of activated sludge (800 ml) and synthetic municipal sewage (1.6 L) with the following composition: 2561 mg/L of sodium acetate as organic carbon source, 400 mg/L of peptone, 250 mg/L of meat extract, 45 mg/L of KH_2PO_4, 200 mg/L of NH_4Cl, 25mg/L of $MgSO_4 \cdot 7H_2O$, 30 mg/L of $CaCl_2 \cdot 2H_2O$, 20 mg/L of $FeSO_4 \cdot 7H_2O$ and 1 mL/L of trace element

solution (Iorhemen et al.,2019). The trace element solution consists of micronutrients, including 0.05 g/L of H_3BO_3, $ZnCl_2$, 0.03 g/L of $CuCl_2$, 0.05 g/L of $MnSO_4 \cdot H_2O$, 0.05 g/L of $(NH4)_6Mo_7O_{24} \cdot 4H_2O$, 0.05 g/L of $AlCl_3$, 0.05 g/L of $CoCl_2 \cdot 6H_2O$, and 0.05 g/L of $NiCl_2$.The influent pH was controlled at 8.2 ± 0.5, while the effluent pH was from 7 to 8. Besides, the synthetic water was stored in a 5-gallon plastic container at the temperature ranging from 20 to 27°C.

250 ml of sludge samples were collected every 7 days (SRT) from the sampling port (above the influent port) to measure MLSS, mixed liquor volatile suspended solids (MLVSS), and sludge volume index (SVI) following Standard Methods (Apha.,1998). Meanwhile, the same volume of fresh sludge must be refilled in the reactor to sustain the culture environment. The initial MLSS/MLVSS concentration of settled sludge was 2246 mg/L and 1797 mg/L, while the SVI30 was 267ml/g in the AGS reactor. The evolution of granule size and morphology was monitored by a stereomicroscope (AmScope, Irvine, CA, US). The initial mean granule size was 200 µm within the first 10 days of the experiment setup. The AGS performance was assessed (Table 3.1) in terms of COD, nitrogen, and phosphorus removal. COD, NH_3-N, NO_2^--N, NO_3^--N, and PO_4^{3-}-P in effluent water samples were measured according to Standard Methods (Apha.,1998). All the wastewater samples were filtered through 0.45 µm glass microfiber filter paper (Whatman VWR, Radnor, PA) prior to water quality analysis (COD and nutrients test). The OLR was 6.77 kg COD/($m^3 \cdot$day).

1 – Feed tank
2 – Feed pump
3 – AGS reactor
4 – Air pump
5 – Air flow controller
6 – Effluent pump
7 – Storage tank
8 – Stirred cell
9 – Beaker on the analytical scale
10 - Nitrogen gas cylinder
11 - pH controller
12 – DO meter
Blue pipeline – water line
Black pipeline – air/nitrogen line
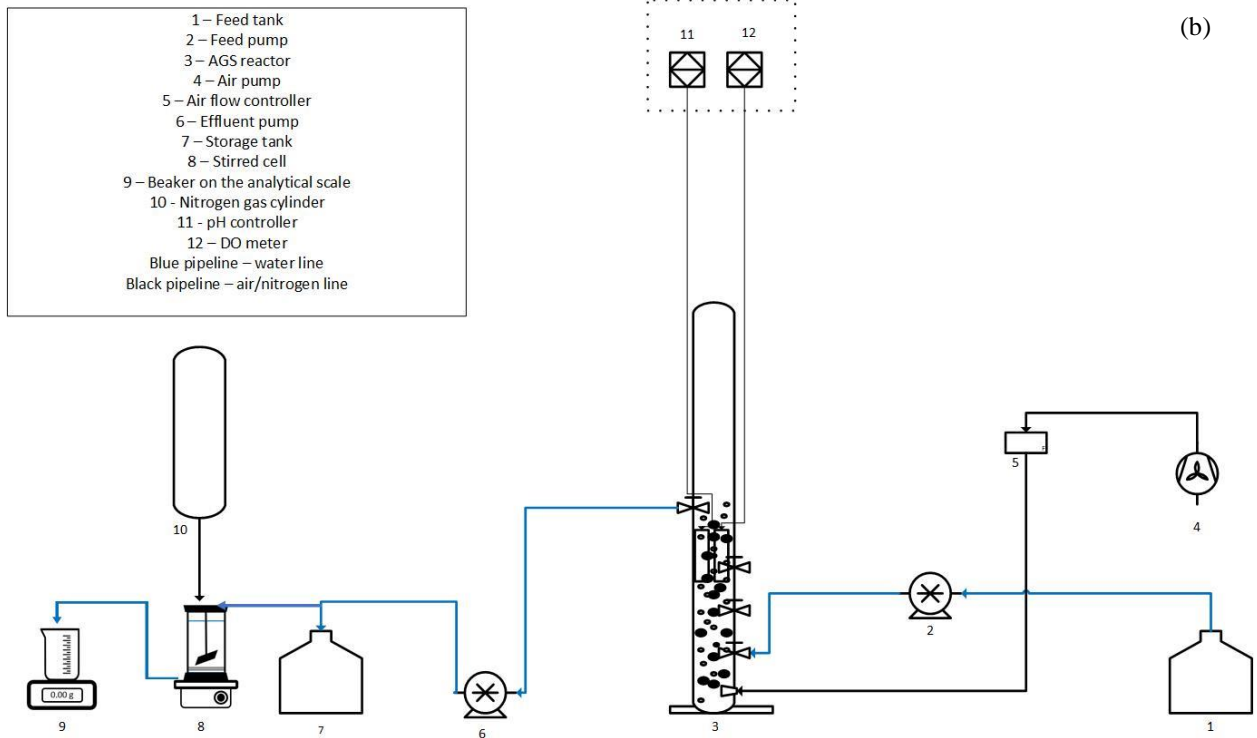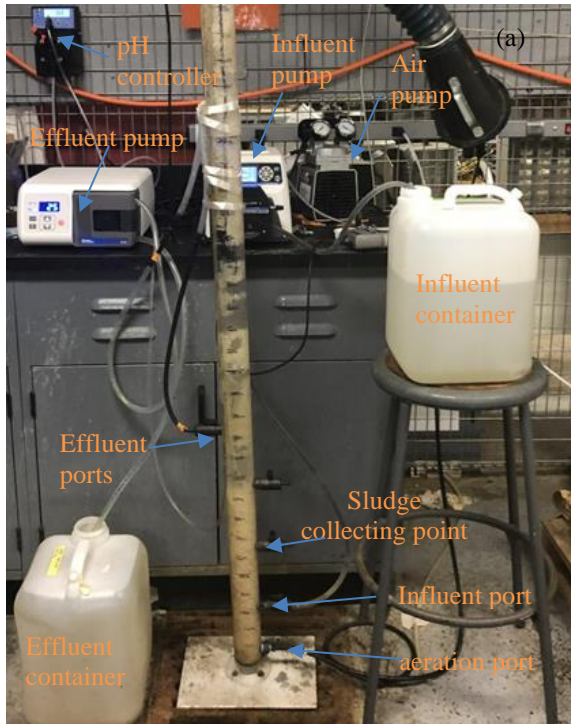
Figure 3.1 *(a)Photo of AGS reactor and (b) schematic design of AGSM*

Table 3.1 *Water quality and sludge analytical methods*

Analytical method	
Parameters	**Methods**
NH_3-N	Nitrogen-Ammonia Reagent Set, TNT, AmVer (Salicylate)
PO_4^{3-}-P	HACH Phosphorus Orthophosphate Test Kit
NO_2^- - N	HACH Nitrate-Nitrite Test Kit Model NI-12
NO_3^- - N	
COD	COD Test Kit 0-150ppm
MLSS/MLVSS	APHA,1998, Standard Methods
PN	Bradford assay
PS	Phenol-sulfuric acid with glucose Method
SVI5, SVI30	APHA,1998, Standard Methods
Particle size distribution in effluent water	Multisizer 3 Coulter Counter
Granule size and morphology	AmScope stereomicroscope

3.2 Water quality and sludge characteristics

Both water quality (e.g., COD and nutrients) and sludge characterization (e.g., MLSS/MLVSS, SVI, and EPS in granules) follow the APHA Standard Methods.

COD analysis relies on the HACH COD test kit. First, the standard calibration curve between absorbance and concentration is prepared by diluting 1000mg/L COD stock solution in series (e.g., 10, 30, 50, 100 mg/L). 2 ml of diluted stock solution is added into each COD test tube. Then, test tubes are placed in the Labnet D1302 AccuBlock Dry block heater (Nurnberg Scientific, Tualatin, OR, US) and heated to 150 °C for 120 min. All the test tubes need to be cooled down prior to absorbance measurements in the Orion AquaMate 8000 UV-Vis spectrophotometer (Thermo Scientific, Waltham, MA, US) at 420 nm. The blank is prepared by adding 2 ml DI water into the test tube, while 2ml filtered samples (via 0.45 um filter paper) are pipetted into the test tube before COD reaction. The rest steps are the same as the COD standard curve preparation. The nutrients tests also require a build-up of the standard curve (e.g., absorbance vs. concentration) before wastewater sample analysis. For example, 0.1 ml of series diluted ammonia standard solutions (up to 50 mg/L) are added into each ammonia test tube, which is fully mixed with salicylate and cyanurate powder packs. It takes a 20-minute waiting time prior to absorbance measurements under the wavelength of 550 nm. 0.1 ml of blank and filtered wastewater samples are pipetted into the test tube, and the rest steps are the same as standard curve preparation. For nitrite/nitrate analysis, 5 ml of series diluted nitrite or nitrate standard solutions, blank or filtered samples are transferred into the test tube, mixing with HACH NitraVer powder. Chemical reaction waiting time for nitrate and nitrite are 1 and 10 minutes, respectively. Finally, the UV-Vis spectrometer illustrates absorbances under the wavelength of 507 nm for nitrite and 410 nm for nitrate. The absorbances correspond to the specific concentrations for the standard curve. The

phosphate analysis requires a mixture of 20 ml of filtered wastewater sample, DI water as blank, or standard solution with HACH phosphate reagent powder. Then, the absorbances are measured via UV-Vis spectrometer under a wavelength of 420 nm after 8 minutes of the chemical reaction.

For MLSS measurements, 40 ml of a well-mixed sample is filtered through a weighed standard 0.45 µm filter, and the residue retained on the filter is dried to a constant weight at 103 °C for overnight. The increase in weight of the filter represents dried residual weight; thus MLSS can be determined by using the difference of mass of dried residuals and aluminum boat with filter paper divided by the sample volume. Then, the sludge sample was further dried in a furnace at 550 °C for MLVSS analysis. Similarly, the MLVSS are reported in mg/L by using the same equation as MLSS. For SVI5 and SVI30 settling test, 250 ml of liquid sludge samples are poured into a 1 L graduated cylinder, and it requires to record the liquid surface level change at 5 minutes and 30 minutes, respectively. SVI is recorded in mg/g by using settled sludge volume (mL/L) divided by MLSS (g/L). For EPS (mg/g VSS) content extraction, centrifuge 50 ml sludge samples two times based on the steps below. The first is to get loose-bounded EPS (LB-EPS), while the second is to gain tight-bounded EPS (TB-EPS). The supernatant is LB-EPS and TB-EPS, which must be extracted before evaluating PS and PN. The PS analysis is based on the glucose, phenol-sulfuric acid method, developed by Dubois in the 1950s (DuBois et al., 1956). On the contrary, the PN analytical method is based on Bradford assay with the bovine serum albumin kit (Bensadoun et al.,1976). To extract EPS, these are the following procedures: 1) sludge sample was centrifuged at 5200 G for 5 min, and the EPS contained in the supernatant was termed as ''loosely bound EPS" (LB-EPS); Meanwhile, take another 45 ml sludge sample and centrifuge at 5200 G for 5 min, and let the supernatant pass through the 0.45 µm filter to obtain "Soluble EPS" (s-EPS); 2) the sludge pellet left in the centrifuge tube was washed three times with deionized water, and

then it was re-suspended in 0.05% NaCl solution to its original volume; and 3) The re-suspended sludge sample was put in a water bath (60 °C) for 30 min, and then centrifuged at 5200G for 30 min, and the EPS contained in the supernatant was termed as ''tightly bound EPS'' (TB-EPS). The experiment follows these procedures to quantify PS via the UV-Vis spectrometer: 1) Add 2 ml glucose solution (for PS standard curve build-up), DI water as blank, or wastewater samples into a colorimetric tube. Then, add 0.08 ml 80% phenol and 5 ml 98% of H2SO4; 2) The tubes are allowed to stand for 10 mins, and then they are shaken and placed in the water bath at 25 °C to 30 °C for 10 to 20 mins; and 3) measure the absorbance via the wavelength of 490 nm. Besides, the procedures for PN measurements are following: 1) 2 ml of standard assay (for PN standard curve build-up), DI water as blank or wastewater samples are mixed with 1.5 ml of Bradford Reagent; and 2) measure the absorbance via the wavelength of 595 nm.

Besides, the evolution of granule size and morphology was monitored by a stereomicroscope every 7 days. Approximately 10 ml of wet granules were poured into a clean petri dish, and then both camera of microscopy and cellphone took photos of the granules. Finally, the AmScope software processed the granule image with a scale. The granules photos are illustrated in the section 4.2.

3.3 Ultrafiltration experiments

Membrane fouling was determined by measuring the flux decline during the filtration of the effluent obtained from the AGS reactor. This measurement was performed using a dead-end, stirred ultrafiltration system (Millipore, Billerica, MA). The filtration unit comprised a glass stirred cell with a membrane area of 45 cm^2. A compressed N$_2$ tank provided the pressure. During the first stage (from Day46 to Day143), the pressure was controlled at 20 psi for both polyethersulfone (PES) and polyvinylidene fluoride (PVDF) membrane. The second stage (Day 150 to Day 217)

applied constant pressure at 20 psi on PVDF, while the pressure increased from 30 to 40 psi with a 10 psi increment each filtration. The purpose was to investigate the filtration performance and fouling effects under various hydrodynamic drag forces as well as different materials. The permeate samples were collected in a beaker which was placed on a digital scale (OHAUS Navigator, NJ). Permeate water flux was calculated from the change in the mass of permeate water as a function of time. Before each fouling experiment, fresh membranes were compacted with DI water until a stabilized permeate water flux was achieved (J_0). The permeability (A_w) of the fresh membrane was determined by

$$J_w = A_w P \tag{1}$$

where J_w is water flux through the membrane, A_w is the apparent water permeability of the membrane and P is the applied hydraulic pressure. Approximately 400 ml of DI water was permeated via the membrane surface when the flux decline was stabilized.

Then fouling experiments were initialized by feeding the AGS effluent into the stirred cell. The applied pressure was kept constant during fouling tests, and the permeate flow rate was continuously recorded. Roughly 400 ml of AGS effluent was filtered through PES and PVDF membrane surface. At the end of each fouling experiment, the fouled membrane was gently removed from the stirred cell and rinsed with DI water for 10 min. After cleaning, the flux of deionized water and membrane pure water permeability was measured again as a measure of flux recovery to determine the fouling reversibility.

To identify membrane fouling mechanism, a combined caking and complete blockage model was applied to describe experimental data. This model accounts for the combined effects of (1) cake layer formation, which occurs when particles accumulate on the membrane surface and enhances resistance to water flow, and (2) pore blockage, which occurs when particles seal off

pore entrance and prevent water flow (Bolton et al.,2006). The model equation was derived from Darcy's law and is described by Eq. 2

$$V = \frac{J_0}{K_b}\left(1 - \exp\left(\frac{-K_b}{K_c J_0^2}\left(\sqrt{1 + 2K_c J_0^2 t} - 1\right)\right)\right) \tag{2}$$

where V is accumulative permeate volume, J_0 is initial permeate flux, K_b is complete blocking constant, K_c is cake filtration constant and t is filtration time. Alternatively, an internal membrane fouling model indicates similar fouling mechanism, which consists of cake layer, pore blocking (e.g., deposition onto the pore mouth), and pore constriction (e.g., deposition within the pores) (H.T. Lay et al., 2021). The model equation was derived from the flux decline curve under the constant pressure condition:

$$\frac{Q}{Q0} = \frac{1}{(1 + \beta Q0Ct)^2}\exp\left(-\frac{\alpha J0t}{1 + \beta Q0Ct}\right) + \int_0^t \frac{\frac{\alpha CJ0}{(1 + \beta Q0Ct)^2}\exp\left(-\frac{\alpha J0t}{1 + \beta Q0Ct}\right)}{Rc/Rm}\,dt \tag{3}$$

where Q is permeate flow rate, Q_0 and J_0 are initial permeate low rate and initial permeate flux, C is concentration of foulant particles, R_c and R_m are cake layer resistance and membrane resistance, α is pore blockage parameter, β is the pore constriction parameter.

The curve fitting tool in MATLAB (Mathworks, Natick, MA) was used to fit the UF data of AGS effluent to the model equation. The coefficient of determination R2 characterizes the quality of the fitting results. $R^2 > 0.95$ (or MSE approaches to zero) is considered as a successful fitting, and a higher value indicates a better fitting (Huang et al.,2020).

3.4 UF membranes

Two commercial UF membranes (MQ and BN) selected for this study were provided by Synder Filtration (Vacaville, CA). Both membranes have the same molecular weight cut-off (MWCO) of 50,000 Da. MQ is made of PES, and BN is made of PVDF. Thus, these two membranes exhibit different physicochemical properties (Table 4.1). All membrane samples were

immersed in deionized water at 4 ℃ after receiving from the manufacturer with the water replaced regularly to prevent membrane damage and to activate (or enlarge) the membrane pores. Interfacial properties of both membranes were characterized as described elsewhere (Jin et al., 2009). Contact angle measurement used the sessile drop method to determine the membrane surface hydrophobicity. A drop of DI water (1 µL) was injected onto the dried membrane surface via the syringe. Then, the air-water-surface contact angle was measured immediately using an optical measurement system (First Ten Angstroms, FTA135, Newark, CA, US). Besides, the membrane surface functional groups were analyzed via Attenuated total reflection - Fourier transform infrared (ATR-FTIR) spectroscopy, using a Nicolet iS50 FTIR spectrometer equipped with an ATR element (42° single-reflection germanium SeagullTM variable angle reflection element). Eight replicate ATR-FTIR spectra were obtained for each membrane type, with each spectrum averaged from 100 scans collected from 400 to 4000 cm^{-1} at 4 cm^{-1} increments. An electrokinetic analyzer determined the membrane surface zeta potential from streaming potential measurement (SurPass, Anton Paar, Austria). The samples were placed on the analyzer using an adjustable gap cell apparatus. The streaming potential of the surface was measured to calculate the zeta potential. The measurement was performed at 10 mM KCl solution with pH ranging from 4 to 9. Membrane surface roughness was determined for dry samples by tapping mode atomic force microscopy (Veeco di Innova, Santa Barbara, CA) in air using a silicon nitride probe. Dried samples were cut into small pieces and placed onto the specimen's holder. Images were taken in the scan size of 5 × 5 µm. The root mean square (RMS) roughness values were calculated for five replicates for each type of membrane. A Helios 650 Ultra Resolution Dual Beam field-emission gun scanning electron microscope (SEM) (ThermoFisher Scientific, Waltham, MA) at an accelerating voltage of 5 kV was used to image the membrane surface. The SEM images were analyzed using Image J for

membrane pore size distribution following the method reported previously (Wickramasinghe et al., 2009).

3.5 Foulant Characterization in Feed Water (AGS Effluent)

The particle size distribution of the feed water (AGS effluent) was characterized using Multisizer 3 Coulter Counter (Beckman Coulter, CA) with an aperture size of 400µm. The actual measurable range was from 8 to 240µm based on the manufacture's instructions. In this experiment, 200 ml of Isoton II solution was applied as the blank solution, while 50% diluted AGS effluent (mixture of 100 ml AGS effluent and 100 ml Isoton II) evaluated the particle size distribution. Moreover, other key parameters were set prior to the measurement, including current at 1600 µA and gain at 2. The noise level measurement adjusted the sizing threshold prior to the size distribution test. As EPSs play a key role in membrane fouling (Wang et al., 2009), EPS composition in feed water was also quantified. EPSs are generally categorized as soluble EPS (s-EPS) and bound EPS (b-EPS). The EPSs in AGS effluent samples were extracted as described elsewhere (Chen et al., 2017). Briefly, the effluent sample was centrifuged at 5200 G for 5 minutes, and then filtered through a 0.45 μm sterile filter to obtain the s-EPS. Next, 0.05% NaCl solution was used to suspend the retentate to its original volume. The re-suspended sample was put in a water bath (60 ℃) for 30 minutes and then centrifuged at 7200 G for 30 minutes. The EPS contained in the supernatant was termed as b-EPS. The extracted s-EPS and b-EPS were analyzed for proteins and polysaccharides as they are the major component of EPS (Iorhemen et al., 2016). Protein concentration was determined using the modified Lowry method with bovine serum albumin as a standard (Bensadoun et al.,1976). Polysaccharide concentration was determined using the phenol-sulfuric acid method with glucose as a standard (DuBois et al., 1956).

Table 3.5 Membrane module/materials and characterization methods

Membrane module/materials and characterization methods	
Parameters	**Instrument**
UF membrane	Synder PES (MQ) and PVDF (BN) flat sheet membranes
UF filtration	Millipore dead-end stirred Cell filtration system; ID at 76mm
Mass change/flux decline	OHAUS Navigator digital scale
Hydrophobicity of membrane surface	FTA135 sensile drop contact angle
Chemical composition on membrane surface	Nicolet iS50 ATR-FTIR
Surface charge	Surpass zeta potential
Surface morphology	SEM (Helios 650) and AFM (Veeco di Innova)

Chapter 4: Results and discussions

4.1 Membrane Characterization

The characteristics of the PES and PVDF membranes are summarized in Table 4.1. Both membranes exhibit negative zeta potentials at pH 7.5±0.2 which is the pH level of AGS effluent (feed water to membrane). PES membrane is more negatively charged and has slightly more hydrophilic surface. This is because that PES membrane contains negatively charged and sulfonic acid groups (Gkotsis et al., 2014). Figure 4.9 shows the ATR-FTIR spectra of both membranes. The characteristic peaks including ethane-sulfonates (836 cm^{-1}) (Kuniaki et al.,1959), symmetric SO$_2$ stretching vibration (1180-1145 cm^{-1}), ether band (1200-1275 cm^{-1}), and benzene ring (1475-1600 cm^{-1}) of PES membrane are clearly observed (Luján-Facundo et al., 2015). In addition, Amide I band (1600-1700 cm^{-1}) and Amide II band (1500-1600 cm^{-1}) (Luján-Facundo et al., 2015) suggest the PES membrane may be chemically modified to introduce additional functional groups. In the FTIR spectra of new PVDF membrane, the adsorption peaks appeared at 840 cm^{-1}, 1070 cm^{-1} and 1167 cm^{-1} were attributed to the CF stretching vibration (Gu et al., 2010). The adsorption band at 1400 cm^{-1} corresponded to CH$_2$ wagging vibration (Rehman et al.,2019). The PVDF membrane exhibited negative surface charge in the test pH range from 7 to 8, due to the preferential adsorption of counter ions (e.g., Cl- and OH-) onto membrane surface (Lettmann et al., 1999). Both surface charge and hydrophilicity can impact UF membrane fouling (Evans et al.,2008; Peng et al., 2004). In general, membrane with more negatively charged and more hydrophilic surface is more resistant to organic and biological fouling. Both membranes have same MWCO of 50, 000 Da. According to pore size estimates from MWCO values reported in the literature (Jawor et al., 2010), both membrane applied in this study had characteristics pore diameters of around 7.0 nm. However, it is worth noting that polymer membranes can have a wide distribution of pore sizes.

PES membrane has less water permeability compared to PVDF although both membranes have same MWCO, indicating that PES membrane has tighter porous structure. The membrane pore size distribution obtained by analyzing skin layer SEM images showed that PES membrane (4.72 ± 1.04 nm) had smaller pores compared to PVDF membrane (5.29 ± 1.79 nm). The AFM derived rms roughness values were 1.5 nm and 13.5 nm for PES and PVDF membranes, respectively.

Table 4.1 *Properties of selected UF membranes*

Membrane	Material	Zeta potential[a] (mV)	Contact angle (°)	RMS rougness (nm)	Permeability (LMH/psi)
MQ	PES	-54.3±0.1	66.6±2.3	1.5	3.4±0.5
BN	PVDF	-28.9±0.3	72.1±2.7	13.5	5.8±0.9

[a] at pH 7.5, 10 mM KCl

4.2 Granule Characteristics

The formation and development of aerobic granular biomass were characterized by SVI and average particle size of the granules during operation. SVI is an index to describe the ability of the biomass to settle, which can reflect the compact structure of the sludge. The profile of SVI showed a declining trend throughout the experiment (Figure 4.1a). After almost 45 days, the SVI value decreased to 50.9 ml/g, exhibiting great sludge setting property. Meanwhile, granules were observed by naked eyes in the reactor. This along with the significantly reduced SVI value indicated that successful granulation from non-granular inoculating sludge was achieved after 45 days of cultivation using synthetic municipal wastewater. Then SVI values continued decreasing and eventually stabilized at approximately 6.5 ± 1.8 ml/g after day 143, exhibiting strong and compact granules were formed. The corresponding SVI_5/SVI_{30} ratio stabilized at 1 after day 143.

This also indicated that complete granulation was successfully achieved in the reactor (Liu et al., 2007).

To further verify the formation of granular sludge in the AGS reactor, sludge samples were observed under the microscopy as shown from Figure 4.2, while the granule size distribution was plotted on Figure 4.1b. As discussed earlier, sludge granules were formed after 45 days of operation and the average diameter of sludge jumped to 2.03 ± 0.03 mm, much larger than the size of inoculated sludge particles (0.26 ± 0.04 mm). Thereafter, granular size increased granularly and mostly maintained in the range of 2.5-2.8 mm after day 143.
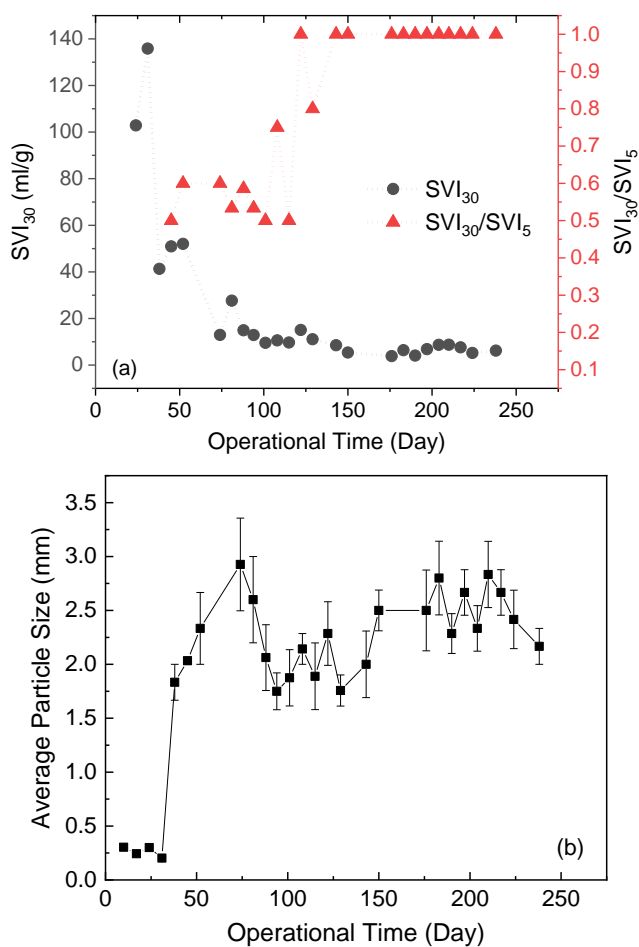
Figure 4.1 *Evaluation of sludge property: (a) settling ability SVI30 and SVI30/SVI5 and (b) average granule size.*
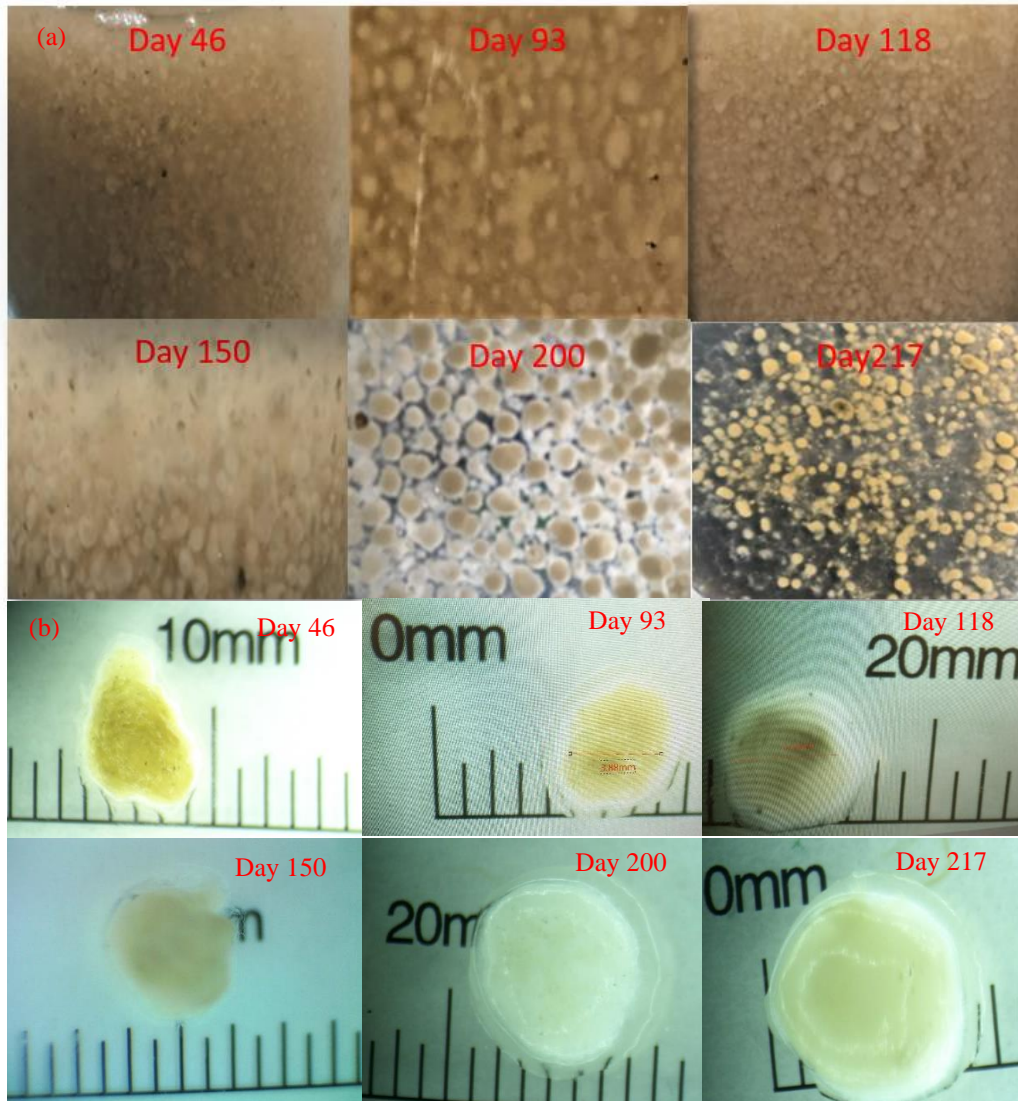
Figure 4.2 *Evolution of granules throughout the culturing period (a)mobile photos and (b)microscopy photos (Note: the sludge samples were in the petri dish while taking mobile photos)*

The MLSS and MLVSS (or sludge) concentrations (Figure 4.3) increased to the peak at 12767 ± 1094 mg/L and 11407 ± 918 mg/L on Day 81, corresponding to the increase of granule size to 2.8mm. Then, the granule size decreased to 2mm while the MLSS and MLVSS concentrations decreased to 6642 ± 199 mg/L and 5839 ± 174 mg/L on Day 118. Generally, the sludge concentration had similar fluctuation trends as the granule size. Besides, the EPS compounds

influenced the granulation significantly. Figure 4.4 illustrated the content of EPS, such as protein and polysaccharides, in the AGS reactor over the period. Besides, the average ratio of TB/LB of EPS was 2.4 since the beginning of the experiment. Tight-bounded EPS had consistently outnumbered loose-bounded EPS in the system since Day24, which suggested more compacted granules were continuously growing from filamentous flocs in the system. Alternatively, the ratio of PN/PS was the other perfect indicator for the granulation (Wang et al., 2006; Zhu et al., 2012). The granules were initially observed by the naked eye in the reactor on Day30. A high ratio of PN/PS (>1) suggested cell hydrophobic interactions dominated in the system due to the hydrophobicity of proteins, aggregating the granulation (Li et al., 2008). Moreover, EPS was tightly correlated with the granule size. Tight-bounded PN initially increased sharply with the increase of granule size, and then it reached a plateau around 125 mg/MLVSS g on Day 143 when the granule diameter was approximately between 2.5 and 2.8 mm. In addition, the increase of EPS content remarkably resulted in a decline of SVI_{30} (Figure 4.1a and Figure 4.4). The SVI_{30} decreased to 8.5 ml/g on Day143 (complete granulation) when the total EPS increased to 270 mg/MLVSS g. This phenomenon suggested that higher EPS content may accelerate the formation of the aerobic granules and improve the settling properties of the aerobic granules (Deng et al.,2016).
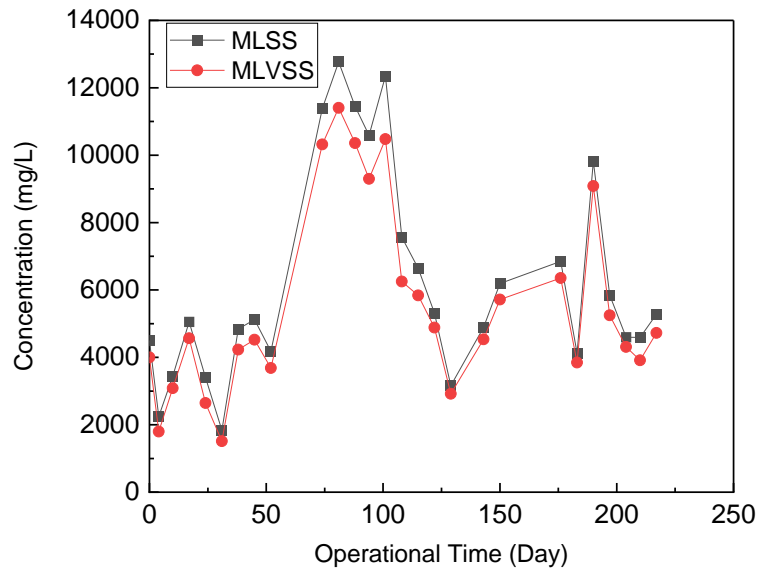
Figure 4.3 *Concentration of MLSS and MLVSS in the sludge sample*
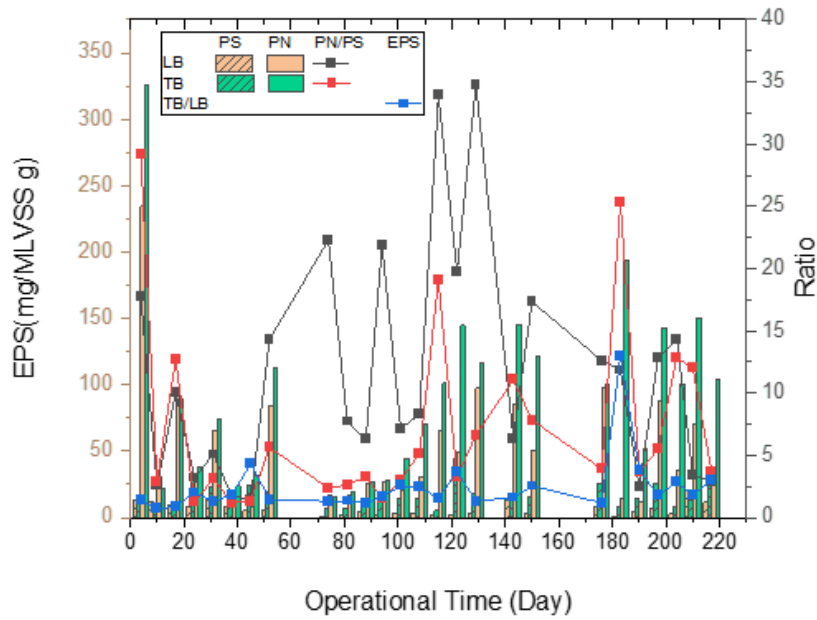
Figure 4.4 *EPS content (PN and PS), ratio of PN/PS, and ratio of TB/LB, in the sludge sample*
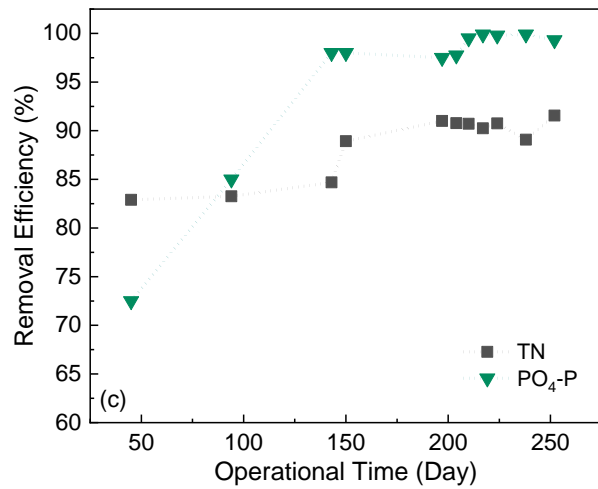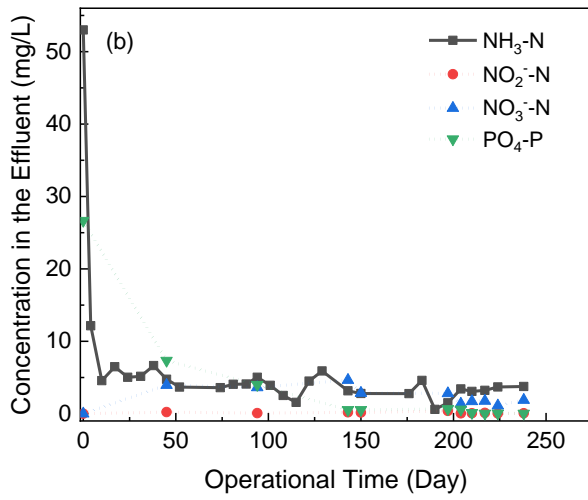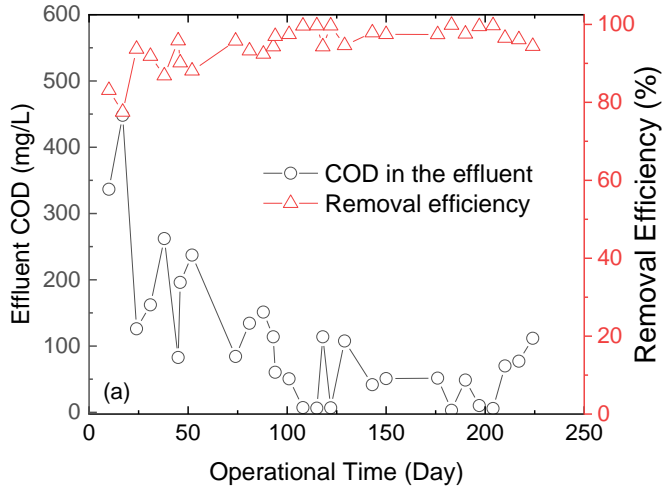
4.3 AGS Reactor Performance

The general performance of the AGS reactor over 8 months of operation is shown in Figure 4.5, in terms of COD, nitrogen and phosphorus. After 74 days of operation, the COD removal remained at a high and stable efficiency of 97.0 ± 2.3% which indicated a good performance of the AGS reactor (Figure 4.5a). The excellent removal efficiency of COD achieved in this study is in good agreement with the results reported in previous literature where organics degradation efficiency was great than 96% (Iorhemen et al.,2019). Besides, the concentration of MLSS and MLVSS in the effluent decreased from 650 and 568 mg/L to 27 and 25 mg/L at the end of the experiment (Day217) as shown from Figure 4.5d, which met the discharge limits of National Pollutant Discharge Elimination System (NPDES) as low as 30 mg/L (Billah et al., 2010).

Nitrogen removal performance in the AGS reactor was also evaluated. After 45 days of operation, 93.4±2.3% of NH$_3$-N removal was achieved with an average effluent NH$_3$-N concentration at 3.5±1.2 mg/L (Figure 4.5b). This is probably due to the presence of *Nitrosomonas* and *Nitrospira* (Iorhemen et al.,2019). NO_2^--N concentration in the effluent was consistently below 0.4 mg/L during the entire operating process (Figure 4.5b), indicating a good nitrification condition formed in the AGS reactor. The NO_3^--N concentration in the effluent increased to 4.1±0.5 mg/L between days 45-143 and then decreased to a low level of 1.8±0.7 mg/L thereafter. The removal of TN remained at above 83% (Figure 4.5c) after 45 days of operation, which demonstrated that a suitable condition for denitrification was formed in the reactor. Simultaneous nitrification and denitrification (SND) is widely reported as a critical factor for efficient nitrogen removal in AGS reactor. Nitrification takes place under aerobic conditions and denitrification takes place under anoxic conditions. Due to the oxygen mass transfer resistance in the compact layered structure of granules, the anoxic zone existed inside granule and the aerobic zone on the outer

surface of granule facilitates the SND process (Yuan et al., 2019). Larger granules are expected to have greater nitrogen removal efficiency. This explains the observation in this study that after 143 days of operation when complete granulation was achieved with SVI_5/SVI_{30} of 1 (Figure 4.1a), TN removal was further enhanced to 90.6±0.8% (Figure 4.5c).

The AGS performance for PO_4^{3-}-P removal is presented in Figure 4.5c. High PO_4^{3-}-P removal of 98.9±1.0 % was achieved after day 143 when granules were fully developed. AGS reactor has been reported to effectively remove PO_4^{3-}-P (Iorhemen et al.,2019). Under anoxic to anaerobic conditions (either inside the anaerobic core of granules or during anaerobic feeding phase), PAO uptake organic substrate and release PO_4^{3-}-P into the water. When aerobic phase is restored, bacteria uptake phosphorus to fulfill their nutrient needs.

In summary, granules were formed on the 45th day. After 143 days of operation, the reactor became predominantly granular with SVI_5/SVI_{30} of 1. At this steady state, the AGS reactor achieved good treatment performance with 97.6±1.7 % removal of COD, 94.3±2.0 % removal of NH_3-N, 90.6±0.8% removal of TN and 98.9±1.0 % removal of PO_4^{3-}-P. The remarkable removal efficiency is attributed to the dense nature of AGS biomass packed with different microbial species (Tay et al., 2009). The membrane fouling is an important factor to affect the performance of the AGSM. In the following sections, the characteristic of membrane fouling during the operation period (before and after complete sludge granulation) will be investigated.
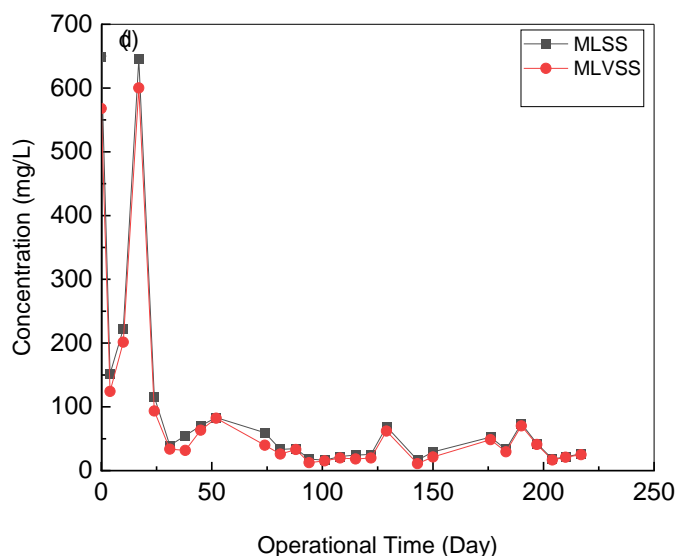
Figure 4.5 *Performance of the AGS reactor: (a) COD in the effluent and COD removal efficiency, (b) concentration of NH_3-N, NO_2^--N, NO_3^--N and PO_4^{3-}-P in the effluent, (c) removal of TN and PO_4^{3-}P，and (d) concentration of MLSS/MLVSS in the effluent*

4.4 Membrane Fouling before Complete Sludge Granulation

Figure 4.6a presents the relative permeate fluxes of PES membrane at the end of fouling experiment and after cleaning with deionized water at Day 46, Day 93, Day 118 (the days before granulation was completed) as well as Day 143 when complete sludge granulation was achieved. In order to focus on the relationship between feed water composition and membrane fouling, all experiments were performed with same initial flux at identical applied pressure of 20 psi. Generally, permeate flux declined due to organic fouling in the AGS effluent that collected before complete sludge granulation (Day 46, Day 93 and Day 118) was similar (25.2-27.6%). Most of the flux decline was reversible by deionized water. This indicates that while flux decline was severe in AGSM, most of the fouling formed with relatively low initial flux (67 ± 5 L/m^2/h) is loosely attached onto membrane surface and thus can be easily washed away by gentle rinsing with

running water. This physical clean method costs much less than chemical clean in real engineering applications. Compared to Day 46 (77.2%) and Day 118 (78.3%), Day 93 had an obviously lower water recovery rate (71.3%) after deionized water cleaning. This can be attributed to the significantly higher contents of both bound and soluble protein in the AGS effluent collected on Day 93 (Figure 4.6b). Protein polymers would bound strongly to the membrane due to their higher stickiness which apparently reduced cleaning efficiency (Iorhemen et al.,2019).

In addition, it was interesting to find that membrane fouling developed more slightly after sludge granulation was completed (Day 143) although Day 143 effluent contained more protein compared to the effluents collected at Day 46 and Day 118. This result combined with the significantly superior effluent quality (lower COD and nutrient concentrations presented in Figure 4.5) after complete sludge granulation indicates that other organic and inorganic component in addition to EPS (particularly protein) may also play a key role in membrane fouling during MBR operation. Systematical characterization of AGS effluent composition and comprehensive elaboration of their fouling mechanisms should be conducted in the future research. However, the current experimental results suggest that after complete sludge granulation was achieved, AGS produced excellent effluent quality which reduced fouling extent and enhanced the effectiveness of physical cleaning in the following membrane filtration process. In the next section, experiments focused on the membrane fouling behavior after complete sludge granulation.
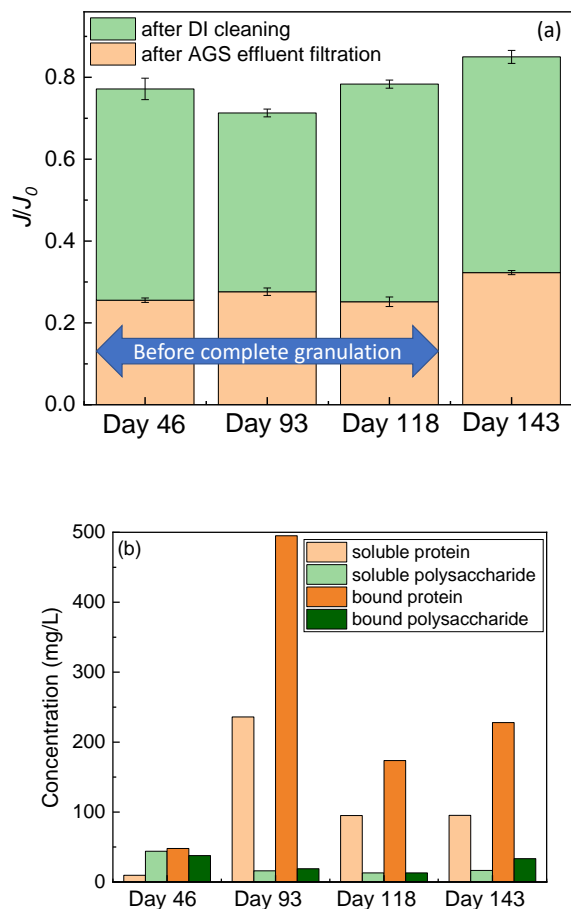
Figure 4.6 *Fouling test before complete sludge granulation (a) Normalized flux of PES membrane at the end of fouling experiment and after cleaning with deionized water, and (b) EPS composition of the AGS effluent collected at Day 46, Day 93, Day 118 and Day 143*

4.5 Membrane Fouling After Complete Sludge Granulation

Membrane fouling is closely related to the concept of critical flux (Nguyen et al.,2019). High permeate flux tends to promote fouling by protein (Jiang et al., 2020), polysaccharide (Mänttäri et al., 2000) and other organic/inorganic component (Cohen et al.,1986; Tang et al., 2007; Hong et al., 1997) in feed water due to the enhanced hydrodynamic drag force (Jiang et al., 2020). In this section, effect of operating pressure (initial permeate flux) on membrane fouling behavior (sustainable operation and fouling reversibility) was investigated after Day 143 when sludge

granulation was completed and good AGS effluent quality was achieved. The critical flux for reversibility was determined.

Figure 4.7a shows the permeate flux decline of PES membrane during fouling test as well as water flux recovered after physical cleaning of the fouled membrane. The initial permeate flux ranged from 59 to 175 LMH and the feed water was AGS effluents at Day 143, Day 150, Day 200 and Day 217, respectively. Clearly, experimental data suggest a rapid initial loss of flux followed by a relatively slow continuous loss of flux over longer time. The initial rapid flux loss could be caused by pore blocking when small particles and EPSs deposited onto the membrane pores. At longer filtration time, the rate of flux decline was greatly reduced under a given pressure when the flux became much lower than the corresponding initial flux. The latter stage could represent the simultaneous effects of pore blocking and cake layer formation as particles and EPSs accumulate inside and on top of the membrane pores and further reduce water permeability (Bolton et al., 2006). Our fouling experimental data fit excellently with the combined caking and complete blockage model (Figure 4.8) (Bolton et al., 2006). According to the definition of the fouling model, the individual contribution of complete blockage and cake layer formation to permeate flux decline can be evaluated from the magnitudes of the fitted parameters K_b and K_c (Table 4.2). For all the fouling experiments in this study, the ratio of $\frac{K_c J_0}{K_b / J_0}$ was much greater than 1, indicating that cake layer formation on membrane surface is the dominant fouling mechanisms. Although the internal membrane fouling model (Figure 4.9 and Table 4.3) indicated the cake layer deposition was the dominating mechanism, the experimental results did not perfectly fit on the thermotical curve. Therefore, combined cake-complete model was more supportive to demonstrate the membrane fouling mechanism. This can be explained by the much larger particle size in AGS effluent (Figure 4.10) compared UF membrane pore size which made it difficult to enter membrane pores and thus

cause pore blocking. Similar results have been achieved by other researchers who reported that pore blockage is less likely to develop in UF membranes (Wang et al., 2018; Charfi et al., 2012). Irrespective of the feed water composition (Figure 4.7b), fouling rate and extend showed an increasing trend as the initial water flux increased (higher operating pressure). It is noteworthy that compared to Day 143, the AGS effluent collected on Day 150 contained similar organic composition except significantly more abundant bound-protein. Day 150 test with initial flux of 92 LMH experienced 12% higher flux decline compared to Day 143 test with initial flux of 60 LMH. This is caused by the combined effect of greater permeation drag force and greater bound protein content in the feed water at Day150. Nevertheless, we noticed that the flux recovered by gentle deionized water flushing appear to be similar for both tests, with recoveries greater than 85%. It is likely that the fouling by AGS effluent could be readily reversible when operating at a low or moderate initial flux. Further increasing initial flux exacerbated flux decline and reduced the effectiveness of physical cleaning. After fouling test on Day 217, only 52% of water flux was recovered. As indicated by the model fitting parameters (Table 4.2), cake layer formation (surface deposition) is the key fouling mechanism. Thus the severer fouling and reduced cleaning efficiency with greater initial flux can be explained by the fact that higher operating pressure caused (1) quicker accumulation of foulants on the membrane surface and (2) more compact cake layer which was harder to be removed by deionized water (Cornehl et al., 2014). The above findings demonstrate the existence of a threshold flux (92LMH) for fouling reversibility when UF membrane is applied to treat AGS effluent. Operating above the threshold flux should be avoided in real applications as the UF performance will be compromised with extensive cake layer formation, leading to irreversible fouling. In contrast, reversible fouling can be achieved when the initial flux is below the critical flux. Consequently, this mode can have significant practical

implication due to the cost savings arising from the elimination of chemical cleaning as well as elongation of membrane lifespan. Membrane fouling in long term run will be investigated to further confirm the sustainability of AGSM process.
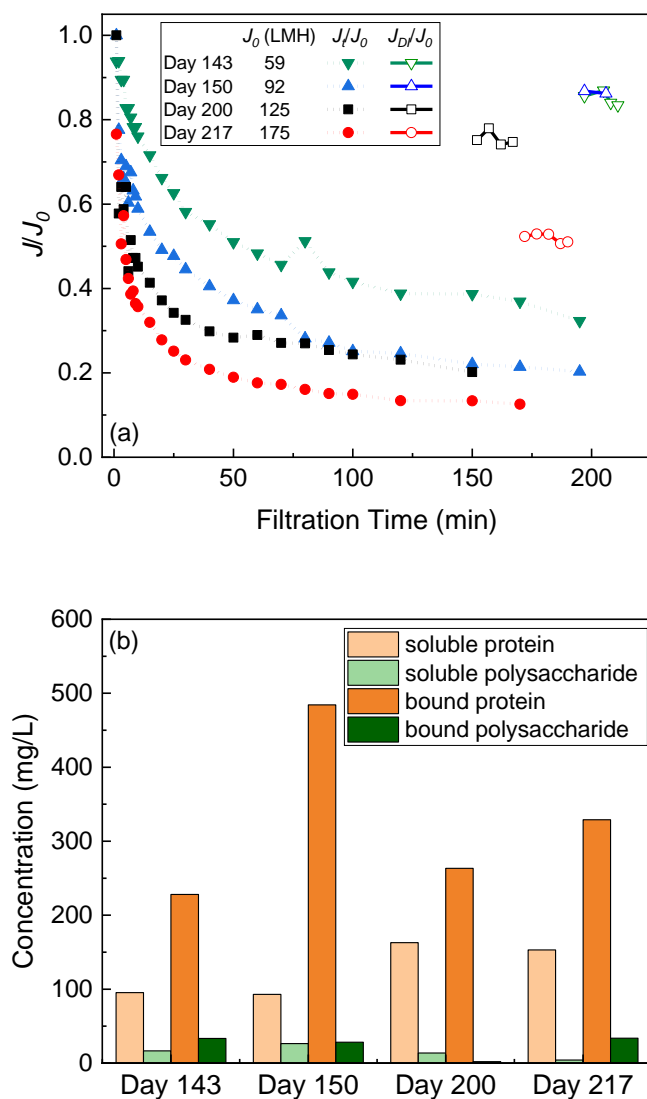
Figure 4.7 *Fouling test after complete sludge granulation (a) Flux behavior of AGS effluent as well as water flux recovery after physical cleaning with PES membrane, and (b) EPS composition of the AGS effluent collected after complete granulation*
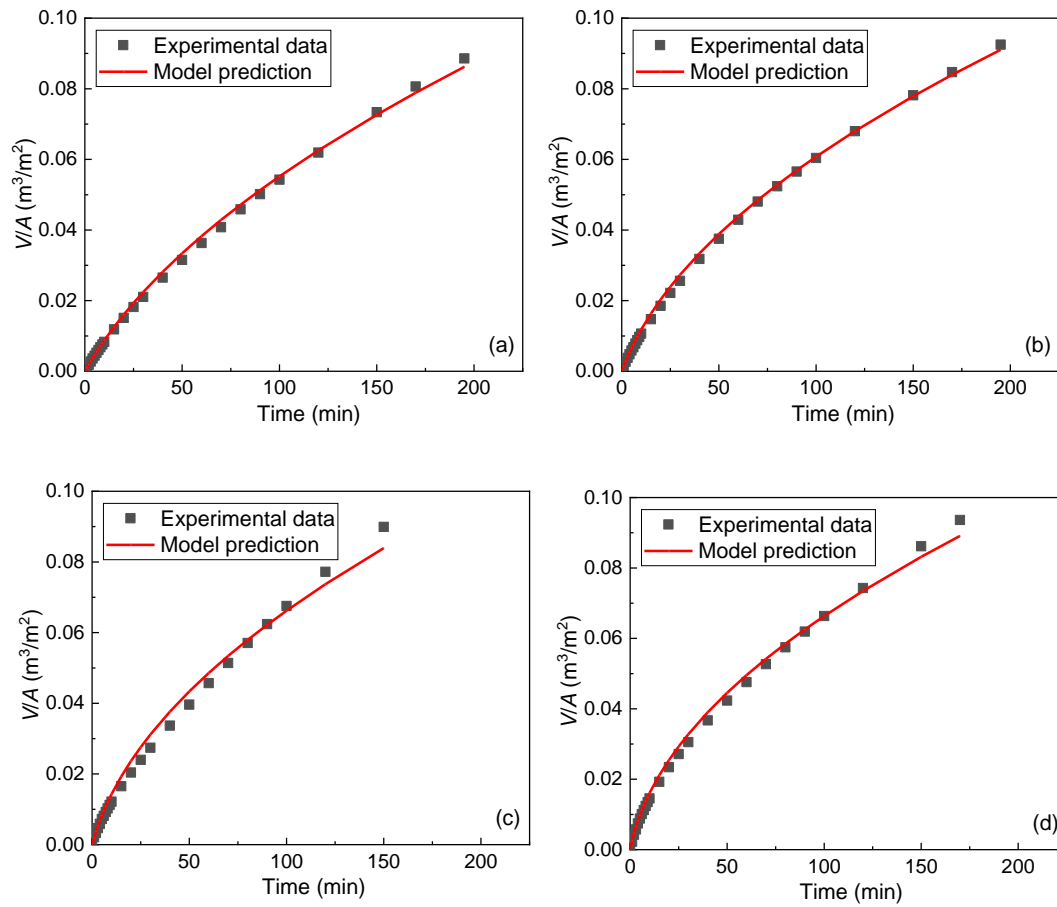
Figure 4.8 *Combined cake-complete model fits for filtration experiments using PES membrane: (a) Day 143 effluent with initial flux of 59 LMH, (b) Day 150 effluent with initial flux of 92 LMH, (c) Day 200 effluent with initial flux of 125 LMH and (d) Day 217 effluent with initial flux of 175 LMH*
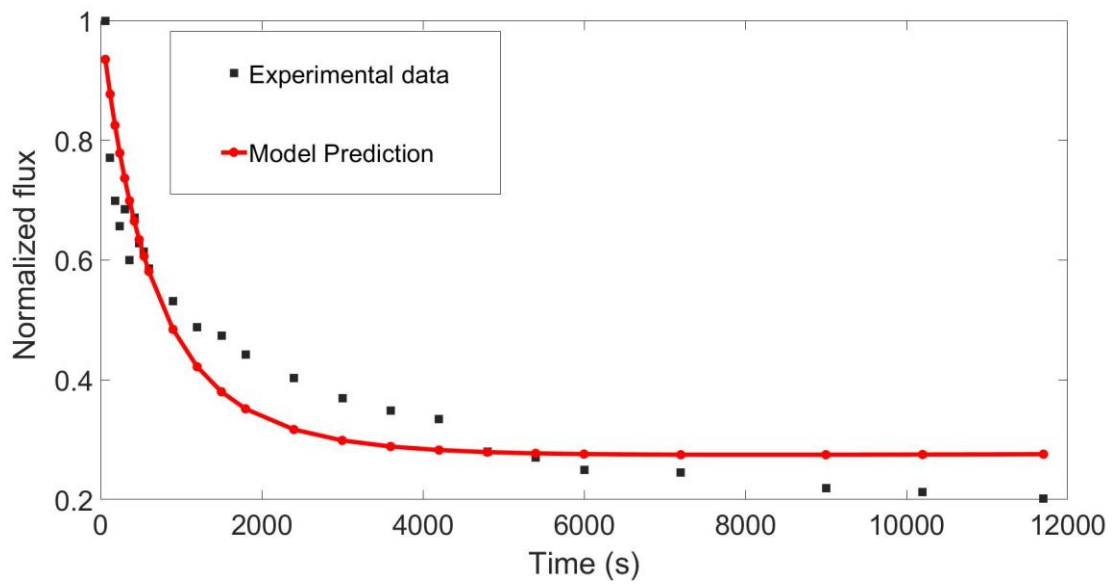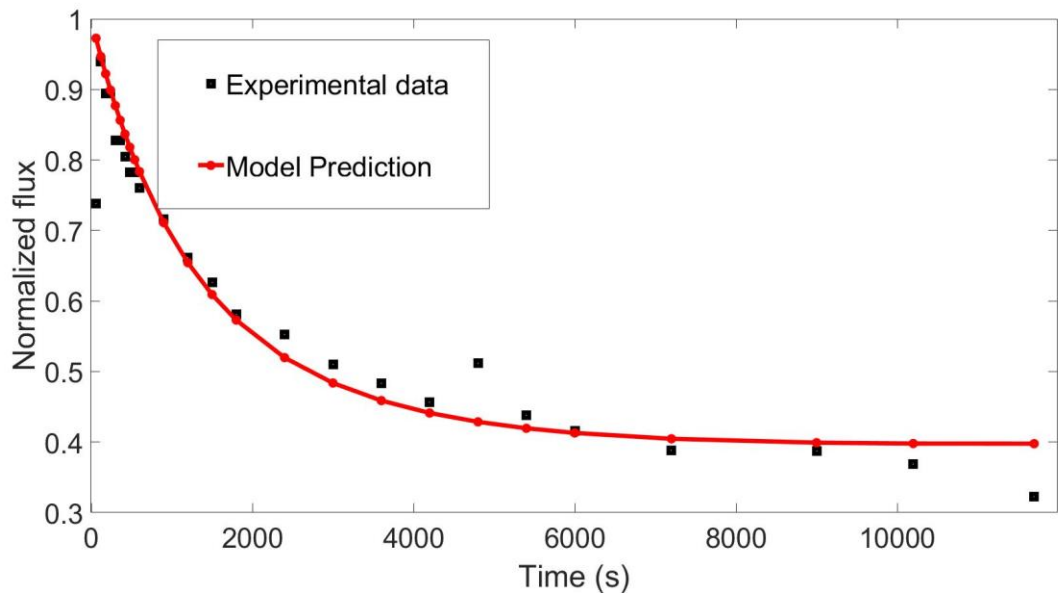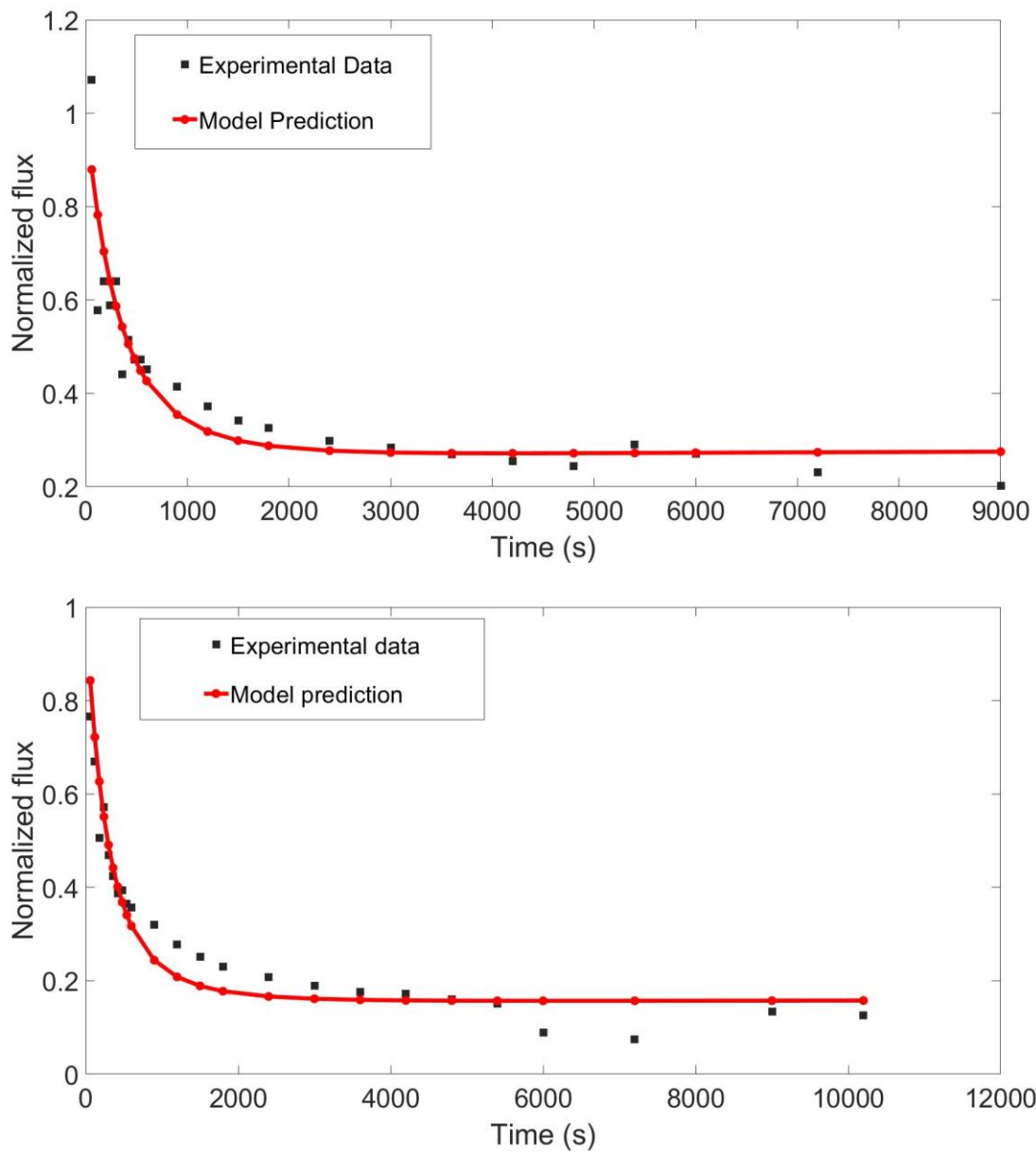
 Figure 4.9 *Internal membrane fouling model fits for filtration experiments using PES membrane: (a) Day 143 effluent with initial flux of 59 LMH, (b) Day 150 effluent with initial flux of 92 LMH, (c) Day 200 effluent with initial flux of 125 LMH and (d) Day 217 effluent with initial flux of 175 LMH*
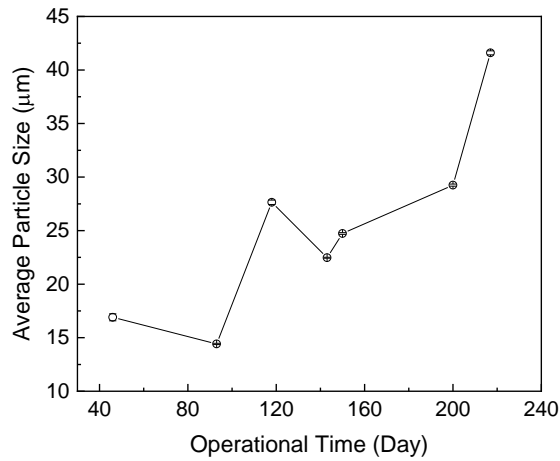
Figure 4.10 *Average particle size in AGS effluent*

Table 4.2 *Fitting results of the combined cake-complete model for the UF process of AGS effluent*

	Model fit error, R^2	Characteristic parameters			
		K_c (s/m^2)	K_b (s^{-1})	$K_cJ_0/(K_b/J_0)$	
Day 143	0.9982	1.73x10^6	2.88x10^{-7}	1622	
Day 150	0.9987	1.96x10^6	2.00x10^{-7}	6408	PES membrane
Day 200	0.9904	1.87x10^6	1.25x10^{-7}	18331	
Day 217	0.9959	2.11x10^6	1.95x10^{-7}	26501	
Day 200	0.9819	2.79x10^6	3.41x10^{-7}	9445	PVDF membrane
Day 217	0.9911	4.32x10^6	5.71x10^{-7}	17911	

Table 4.3 *Fitting results of the internal membrane fouling model for the UF Process of AGS effluent*

	Model fit fit error, MSE	Characteristic parameters			
		α, m2/kg	β, m2/kg	Rc/Rm	
Day 143	0.001	49.12	43.32	1.53	
Day 150	0.006	53.82	16.27	3.39	
Day 200	0.0039	80.68	29.57	3.30	PES Membrane
Day 217	0.0033	94.44	36.93	5.73	
Day 200	0.0018	125.00	76.15	3.17	PVDF Membrane
Day 217	0.0032	143.20	37.37	8.31	

4.6 Effect of Membrane Materials on Membrane Fouling

PES and PVDF polymeric membranes are commonly used in ultrafiltration applications in the water and wastewater market. PES membranes have the advantage of good UF rating and outstanding chemical tolerance. PVDF membranes are excellent for strength and flexibility with very high chlorine tolerance (Pearce et al., 2007). Therefore, in this section, filtration experiments were performed with two membranes made by PES and PVDF. The behavior of these two UF membranes were evaluated and compared in terms of flux decline after filtration of AGS effluent and cleaning efficiency of deionized water flushing.

During UF experiments, the major fouling in AGS effluent is suspended particles which are much larger than the membrane pores and thus they are almost completely rejected by UF membrane. Turbidity rejections (after 400 ml of AGS effluent was filtered) is 93.4-95.6 % for PES and 91.7-93.1 % for PVDF, respectively. PES rejection was consistently higher than PVDF, because PES membrane had tighter porous structure. Figure 4.11 presents the permeate flux decline during fouling test as well as water flux recovered after deionized water cleaning for PES and PVDF membranes on (a) Day 200 with initial water flux at 125 LMH and (b) Day 217 with initial water flux at 175 LMH. For both days, the rate and extent of flux decline was greater for PVDF membrane than for PES membrane. After deionized water flushing, the cake layer with loose structure was lifted up and permeability was recovered to some extent. Clearly, PES membrane demonstrated much higher water recovery (less irreversible fouling) than PVDF membrane. Figure 4.12 shows ATR-FTIR spectra of virgin and deionized water cleaned membrane after fouling experiments. On Day 200 with initial water flux at 125 LMH, there is no visible difference of peaks between virgin and cleaned membrane, indicating that a large amount of the foulants have been removed by physical cleaning. On day 217 with initial water flux at 175 LMH,

there is an observable enhancement of the peaks in the range of 3450-3200 cm-1 and 3080-2850 cm-1 for both membranes. The notably increased spectral intensity in these regions suggests irreversible fouling is caused by hydroxyl (or amino group) compounds (Rahman et al., 2018). In addition, cleaned PVDF membrane showed slightly enhanced peak at 1650 cm-1, corresponding to amide I band which originates predominantly from the C=O stretching vibration of peptide groups (Salgin et al.,2006). This indicates that the major irreversible fouling on PVDF membrane is caused by protein which has inherent flexibility and is the dominating EPS component in the AGS effluent. Previous study reported that PVDF membrane could induce the rapid structural change of proteins after initial protein adsorption onto the membrane because of the hydrophobic attraction (Salgin et al.,2006; Zhao et al.,2014). The deformed structure would facilitate the following adsorption behavior and result in a fast adsorption rate for protein onto the membrane surface (Liu et al., 2020; Du et al., 2014). This may explain the greater fouling potential and lower cleaning efficiency of PVDF membrane when treating AGS effluent.

As mentioned above, the combined cake-complete model provided best fit of all filtration data (Figures 4.8 and 4.13). The cake layer formation on membrane surface is the dominant fouling mechanisms, suggested by the extremely high value of $\frac{K_c J_0}{K_b / J_0}$. Under the same filtration conditions (same AGS effluent and initial water flux), PVDF membrane always had greater K_c value than PES membrane, indicating that more cake layer was formed on PVDF membrane. This agrees with a previous comparative study which found that suspended particles deposition onto PVDF membrane were more than that onto PES membrane in submerged MBR to treat synthetic domestic wastewater (Zhu et al.,2009). The different fouling behavior and cleanability between PVDF and PES membranes could be attributed to membrane properties and chemistry (Luján-Facundo et al., 2015; Vatanpour et al., 2014). First, PES membrane is more negatively charged compared to

PVDF membrane. This leads to a stronger repulsion between negatively charged particles and PES membrane, preventing particles deposition if the repulsion is greater than van der Waals attraction. Furthermore, due to the strong repulsion force, the deposited cake layer is relatively easily to be lifted up by hydraulic flushing. Second, AFM derived rms surface roughness data confirm PVDF is a bit rougher than PES membrane (Table 4.1). Past theoretical studies suggested nano-scale surface roughness dramatically reduces electrostatic double layer repulsion between membrane and colloidal particles and causes a greater adhesion of foulant onto membrane (Hoek et al., 2003 and 2006). Thus, the foulants in AGS effluent preferentially accumulate onto the relatively rougher and less negatively charged PVDF membrane.
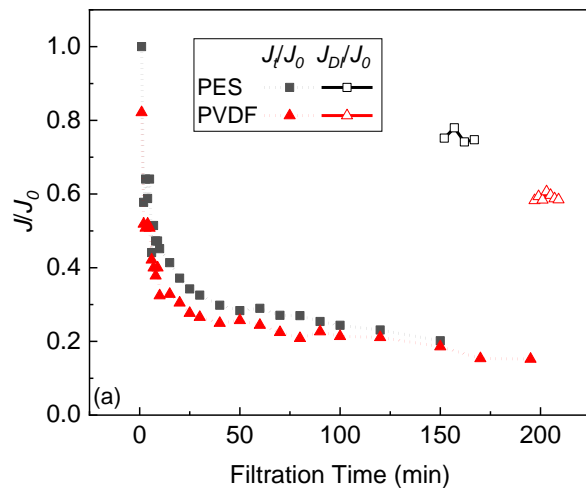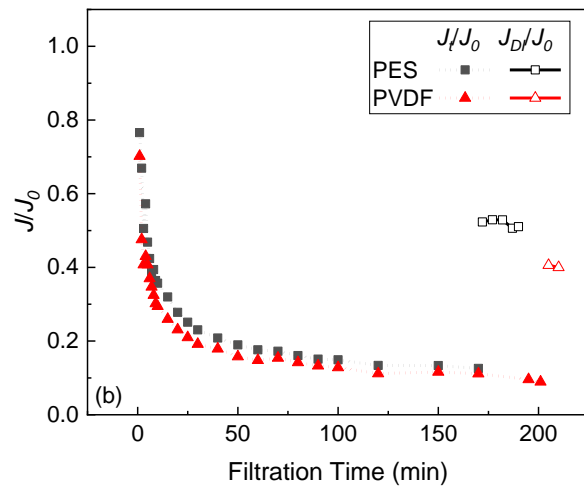
Figure 4.11 *Flux decline during AGS effluent filtration experiments with PES and PVDF membranes as well as permeability recovery after water rinsing on (a) Day 200 and (b) Day 217*
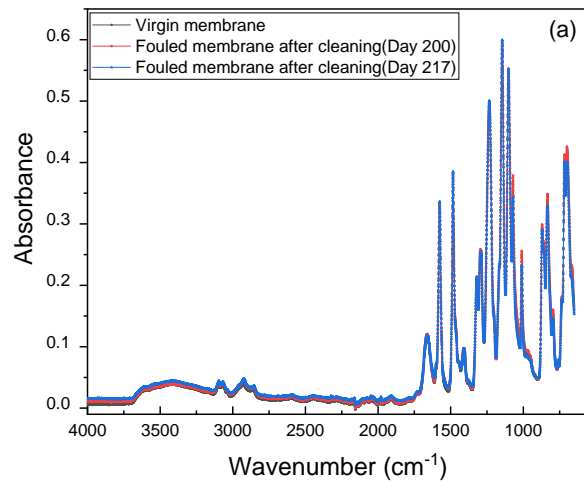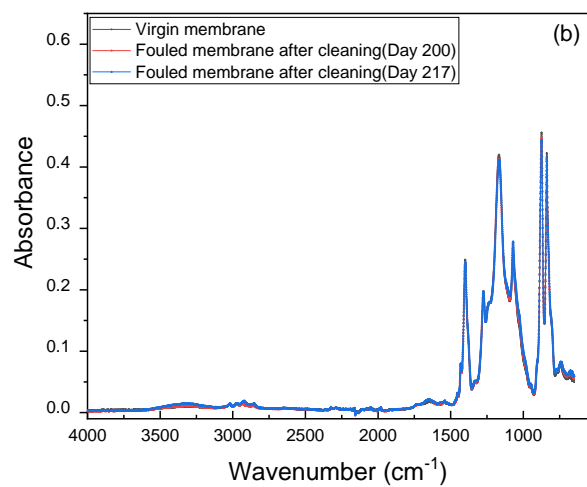
Figure 4.12 *FTIR spectra of virgin (black) and fouled membrane after deionized water cleaning at Day 200 (red) and Day 217 (blue): (a) PES membrane and (b) PVDF membrane*
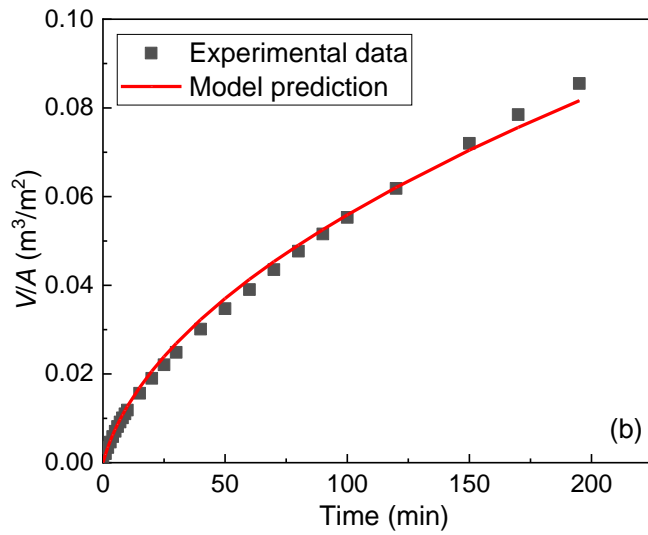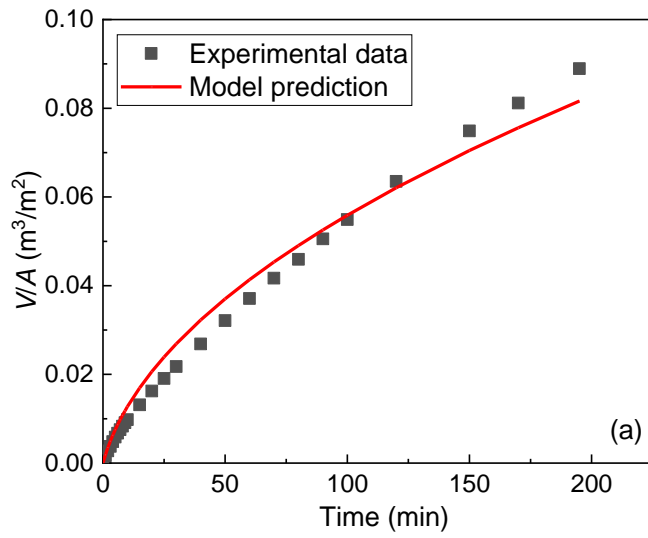
Figure 4.13 *Combined cake-complete model fits for filtration experiments using PVDF membrane: (a) Day 200 effluent with initial flux of 125 LMH and (b) Day 217 effluent with initial flux of 175 LMH*
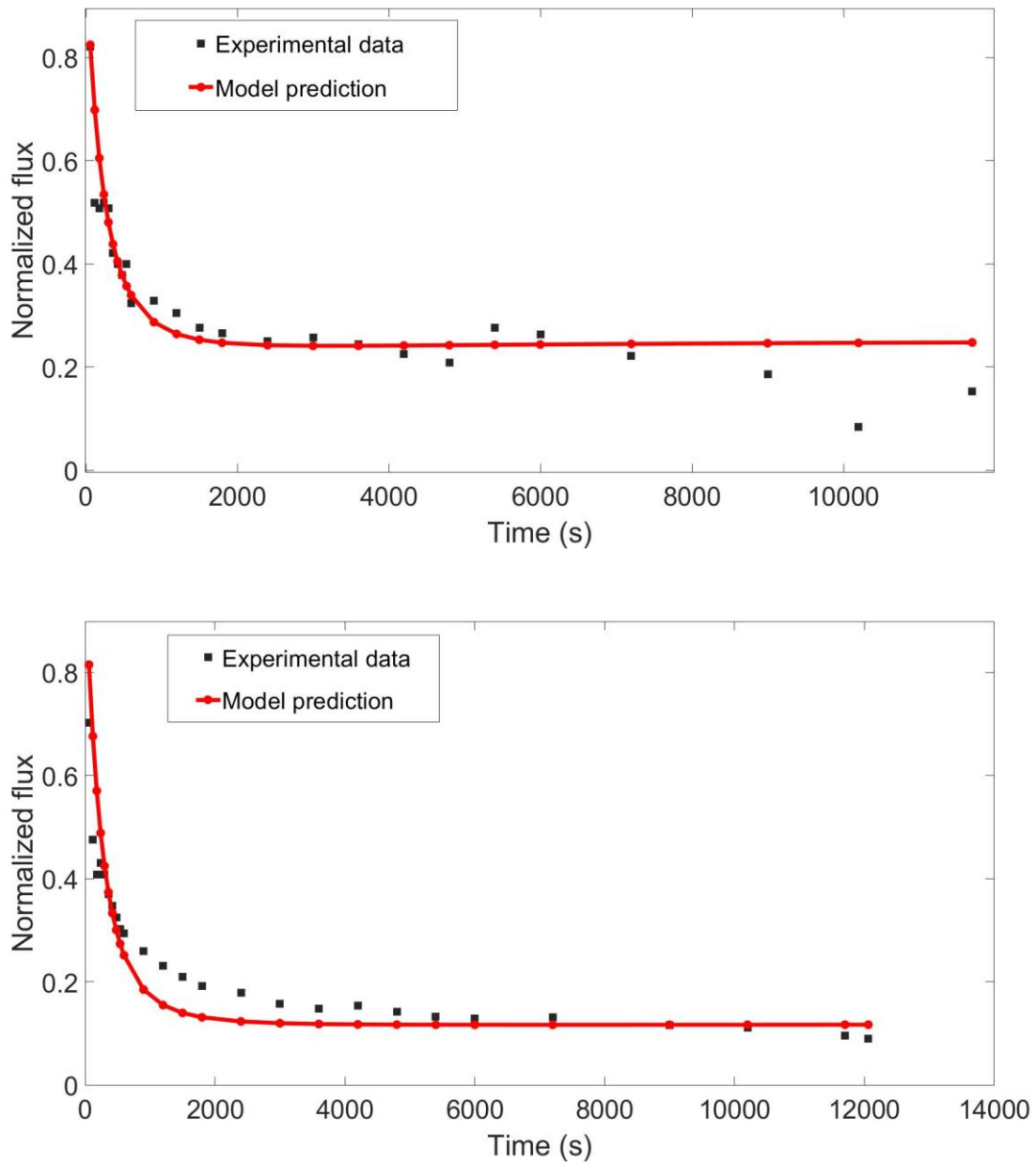
Figure 4.14 *Internal membrane fouling model fits for filtration experiments using PVDF membrane: (a) Day 200 effluent with initial flux of 125 LMH and (b) Day 217 effluent with initial flux of 175 LMH*

Chapter 5: Conclusions and Recommendations

5.1 Conclusions

This study investigated the effects of granule evolution, initial water flux and membrane material on membrane fouling behavior, and reversibility in a side-stream AGSM. After complete sludge granulation was achieved, the AGS reactor demonstrated high removal efficiencies for organic matters and nutrients. UF treatment of the AGS effluent led to less foulant deposition onto the membrane due to the high effluent quality compared to the filtration before complete granulation. For the first time, integrating the experimental filtration data with the combined cake-complete model confirmed that cake layer formation is the dominating fouling mechanism during ultrafiltration of AGS effluent. PES membrane outperformed the PVDF membrane in terms of fouling control, which indicates that the PES membrane might be favored for practical applications of the AGSM technology. This study confirmed the existence of a threshold flux for fouling reversibility. After simple water flushing, high restoration of water flux (>85%) was achieved with the PES membrane at an operation below the threshold flux (92 LMH), which is critical to minimize chemical cleaning. Further studies on the physical cleaning conditions optimization (e.g., shear stress, temperature, and time) are necessary.

5.2 Recommendations

Based on the results obtained from this thesis, it is imperative to investigate the following research area further:

- The AGS reactor can be integrated with an MBR system instead of a stirred cell in the current study. Instead of a constant pressure mode, the flux can be controlled constantly using a digital peristaltic pump and flow meter. Meanwhile, the pressure gauge will be

installed to monitor the TMP variation during the experiment. In this case, the increase of TMP indicates the membrane fouling and when to clean the membrane surface.

- The compositions of EPS in the granules have high adsorption capacity to the emerging contaminants such as pharmaceutical and personal care products (PPCPs). It will be interesting to study further the removal efficiency and its mechanism via AGS and AGSM. In addition, will there be adverse effects on the nutrients removal if PPCPs are present in the system? PPCPs, such as triclosan and ciprofloxacin, may potentially affect nutrient removal efficiency. For instance, most activity enzymes (e.g., nitrite reductase and polyphosphate kinase) towards ammonia and phosphorous removal were inhibited during the occurrence of ciprofloxacin (Wang et al., 2017; Wu et al., 2021; Motlagh et al., 2015). In addition, the abundances of phosphate accumulating organisms (PAOs) and denitrifying bacteria were significantly decreased by the presence of ciprofloxacin. Similarly, the lipophilic triclosan may uptake the volatile fatty acid (VFA), which is an energy for PAOs during the enhanced biological phosphorus removal (EBPR) (Dong et al., 2021; McMurry et al., 1998). Thus, triclosan and PAOs will compete and affect the removal efficiency of nutrients.

- The recycling and reuse of granules meet the trends of environmental sustainability. Instead of dumping granules at SRT, valuable compounds can be extracted from the granules. Alginate-like exopolysaccharides (ALE), a polymer or gel liquid, can be extracted from the granules based on current technologies. ALE can be utilized in the chemistry, paper, textile industries, flame retardant materials, and soil enhancers in agriculture. That will be interesting to study the methods to enhance the ALE harvest as well as the acceleration of granulation. Although some researchers have indicated that

increasing salinity (by using different Na^+ or Ca^{2+} concentrations) may enhance the ALE

recovery rate, those early-stage studies have not elucidated the mechanisms clearly (Lin

et al., 2013; Meng et al.,2019).

References

Ab Halim, M. H., Anuar, A. N., Jamal, N. S. A., Azmi, S. I., Ujang, Z., & Bob, M. M. (2016). Influence of high temperature on the performance of aerobic granular sludge in biological treatment of wastewater. Journal of Environmental Management, 184, 271-280.

Abdel-Karim, A., Gad-Allah, T. A., El-Kalliny, A. S., Ahmed, S. I., Souaya, E. R., Badawy, M. I., & Ulbricht, M. (2017). Fabrication of modified polyethersulfone membranes for wastewater treatment by submerged membrane bioreactor. Separation and Purification Technology, 175, 36-46.

Adav, S. S., Lee, D.-J. (2008). Extraction of extracellular polymeric substances from aerobic granule with compact interior structure. J. Hazard. Mater., 154(1-3), 1120-1126.

Apha, A. W. W. A. (1998). Standard methods for the examination of water and wastewater, 20. Washington, DC: American Public Health Association.

Awang, N. A., & Shaaban, M. G. (2016). Effect of reactor height/diameter ratio and organic loading rate on formation of aerobic granular sludge in sewage treatment. International Biodeterioration & Biodegradation, 112, 1-11.

Bensadoun, A., & Weinstein, D. (1976). Assay of proteins in the presence of interfering materials. Analytical biochemistry, 70(1), 241-250.

Beun, J. J., Van Loosdrecht, M. C. M., & Heijnen, J. J. (2002). Aerobic granulation in a sequencing batch airlift reactor. Water Research, 36(3), 702-712.

Bolton, G., LaCasse, D., & Kuriyel, R. (2006). Combined models of membrane fouling: development and application to microfiltration and ultrafiltration of biological fluids. Journal of Membrane Science, 277(1-2), 75-84.

Brepols, C. (2011). Operating Large Scale Membrane Bioreactors for Municipal Wastewater Treatment. IWA Publishing, UK.

Buer, T., & Cumin, J. (2010). MBR module design and operation. Desalination, 250(3), 1073-1077.

Carta, F., Beun, J. J., Van Loosdrecht, M. C. M., & Heijnen, J. J. (2001).Simultaneous storage and degradation of PHB and glycogen in activated sludge cultures. Water research, 35(11), 2693-2701.

Chang, I. S., Le Clech, P., Jefferson, B., & Judd, S. (2002). Membrane fouling in membrane bioreactors for wastewater treatment. Journal of environmental engineering, 128(11), 1018-1029.

Charfi, A., Amar, N. B., & Harmand, J. (2012). Analysis of fouling mechanisms in anaerobic membrane bioreactors. Water research, 46(8), 2637-2650.

Chaudhry, R.M., Nelson, K.L., Drewes, J.E. (2015). Mechanisms of pathogenic virus removal in a full-scale membrane bioreactor. Environ. Sci. Technol. 49 (5), 2815–2822.

Chen, C., Bin, L., Tang, B., Huang, S., Fu, F., Chen, Q., ... & Wu, C. (2017). Cultivating granular sludge directly in a continuous-flow membrane bioreactor with internal circulation. Chemical Engineering Journal, 309, 108117.

Chen, H., Zhou, S., & Li, T. (2010). Impact of extracellular polymeric substances on the settlement ability of aerobic granular sludge. Environmental technology, 31(14), 1601 1612.

Chen, M. Y., Lee, D. J., & Tay, J. H. (2007). Distribution of extracellular polymeric substances in aerobic granules. Applied Microbiology and Biotechnology, 73(6), 1463 1469.

Chabaliná, L. D., Pastor, M. R., & Rico, D. P. (2013). Characterization of soluble and bound EPS obtained from 2 submerged membrane bioreactors by 3D-EEM and HPSEC. Talanta, 115, 706-712.

Cohen, R. D., & Probstein, R. F. (1986). Colloidal fouling of reverse osmosis membranes. Journal of Colloid and Interface Science, 114(1), 194-207.

Cornehl, B., Overbeck, A., Schwab, A., Büser, J. P., Kwade, A., & Nirschl, H. (2014). Breakage of lysozyme crystals due to compressive stresses during cake filtration. Chemical Engineering Science, 111, 324-334.

Cydzik-Kwiatkowska, A. (2021). Biopolymers in Aerobic Granular Sludge—Their Role in Wastewater Treatment and Possibilities of Re-Use in Line with Circular Economy. Energies, 14(21), 7219.

De Kreuk, M. V., & Van Loosdrecht, M. V. (2004). Selection of slow growing organisms as a means for improving aerobic granular sludge stability. Water Science and Technology, 49(11-12), 9-17.

De Luca, G., Sacchetti, R., Leoni, E., Zanetti, F. (2013). Removal of indicator bacteriophages from municipal wastewater by a full-scale membrane bioreactor and a conventional activated sludge process: implications to water reuse. Bioresource technology, 129, 526 531.

De Sousa Rollemberg, S. L., de Oliveira, L. Q., Barros, A. R. M., Melo, V. M. M., Firmino, P. I. M., & dos Santos, A. B. (2019). Effects of carbon source on the formation, stability, bioactivity and biodiversity of the aerobic granule sludge. Bioresource technology, 278, 195-204.

De Sousa Rollemberg, S. L., Ferreira, T. J. T., Firmino, P. I. M., & Dos Santos, A. B. (2020). Impact of cycle type on aerobic granular sludge formation, stability, removal mechanisms and system performance. Journal of environmental management, 256, 109970.

Del Re, B., Sgorbati, B., Miglioli, M., & Palenzona, D. (2000). Adhesion, autoaggregation and hydrophobicity of 13 strains of Bifidobacterium longum.Letters in applied microbiology, 31(6), 438-442.

Deng, S., Wang, L., & Su, H. (2016). Role and influence of extracellular polymeric substances on the preparation of aerobic granular sludge. Journal of environmental management, 173, 49-54.

Deowan, S. A., Galiano, F., Hoinkis, J., Johnson, D., Altinkaya, S. A., Gabriele, B., ... & Figoli, A. (2016). Novel low-fouling membrane bioreactor (MBR) for industrial wastewater treatment. Journal of membrane science, 510, 524-532.

Di Bella, G., & Torregrossa, M. (2013). Simultaneous nitrogen and organic carbon removal in aerobic granular sludge reactors operated with high dissolved oxygen concentration. Bioresource technology, 142, 706-713.

Dong, X., He, Y., Peng, X., & Jia, X. (2021). Triclosan in contact with activated sludge and its impact on phosphate removal and microbial community. Bioresource Technology, 319, 124134.

Du, P., Zhao, J., Mashayekhi, H., & Xing, B. (2014). Adsorption of bovine serum albumin and lysozyme on functionalized carbon nanotubes. The Journal of Physical Chemistry C, 118(38), 22249-22257.

Du, X., Shi, Y., Jegatheesan, V., & Haq, I. U. (2020). A review on the mechanism, impacts and control methods of membrane fouling in MBR system.Membranes, 10(2), 24.

Dubois, M., Gilles, K. A., Hamilton, J. K., Rebers, P. T., & Smith, F. (1956). Colorimetric method for determination of sugars and related substances. Analytical chemistry, 28(3), 350-356.

Evans, P. J., Bird, M. R., Pihlajamäki, A., & Nyström, M. (2008). The influence of hydrophobicity, roughness and charge upon ultrafiltration membranes for black tea liquor clarification. Journal of Membrane Science, 313(1-2), 250   262.

Franca, R. D., Pinheiro, H. M., van Loosdrecht, M. C., & Lourenço, N. D. (2018). Stability of aerobic granules during long-term bioreactor operation. Biotechnology advances, 36(1), 228-246.

Fu, W., Hua, L., & Zhang, W. (2017). Experimental and modeling assessment of the roles of hydrophobicity and zeta potential in chemically modified poly (ethersulfone) membrane fouling kinetics. Industrial & Engineering Chemistry Research, 56(30), 8580-8589.

Gao, W., Liang, H., Ma, J., Han, M., Chen, Z. L., Han, Z. S., & Li, G. B. (2011). Membrane fouling control in ultrafiltration technology for drinking water production: A review. Desalination, 272(1-3), 1-8.

Giesen, A., de Bruin, L.M.M., Niermans, P.P., and van der Roest, H.F. (2013). Advancements in the application of aerobic granular biomass technology for sustainable treatment of wastewater. Water Practice & Technology 8 (1), 47-54.

Giesen, A., Loosdrecht, M. V., Pronk, M., Robertson, S., & Thompson, A. (2016).Aerobic Granular Biomass Technology: recent performance data, lessons learnt and retrofitting conventional treatment infrastructure. Proceedings of the Water Environment Federation, 2016(11), 1913-1923.

Gkotsis, P. K., Banti, D. C., Peleka, E. N., Zouboulis, A. I., & Samaras, P. E. (2014). Fouling issues in membrane bioreactors (MBRs) for wastewater treatment: major mechanisms, prevention and control strategies. Processes, 2(4), 795-866.

Gu, S., He, G., Wu, X., Hu, Z., Wang, L., Xiao, G., & Peng, L. (2010). Preparation and characterization of poly (vinylidene fluoride)/sulfonated poly (phthalazinone ethersulfone ketone) blends for proton exchange membrane. Journal of applied polymer science, 116(2), 852-860.

Guo, W., Ngo, H. H., & Li, J. (2012). A mini-review on membrane fouling. Bioresource technology, 122, 27-34.

Han, M. J., Baroña, G. N. B., & Jung, B. (2011). Effect of surface charge on hydrophilically modified poly (vinylidene fluoride) membrane for microfiltration. Desalination, 270(1-3), 76-83.

He, Q., Song, Q., Zhang, S., Zhang, W., & Wang, H. (2018). Simultaneous nitrification, denitrification and phosphorus removal in an aerobic granular sequencing batch reactor with mixed carbon sources: reactor performance, extracellular polymeric substances and microbial successions. Chemical Engineering Journal, 331, 841-849.

He, Q., Song, J., Zhang, W., Gao, S., Wang, H., & Yu, J. (2020). Enhanced simultaneous nitrification, denitrification and phosphorus removal through mixed carbon source by aerobic granular sludge. Journal of hazardous materials, 382, 121043.

Hoek, E. M., & Agarwal, G. K. (2006). Extended DLVO interactions between spherical particles and rough surfaces. Journal of Colloid and Interface science, 298(1), 50-58.

Hoek, E. M., Bhattacharjee, S., & Elimelech, M. (2003). Effect of membrane surface roughness on colloid− membrane DLVO interactions. Langmuir, 19(11), 4836-4847.

Hong, S., & Elimelech, M. (1997). Chemical and physical aspects of natural organic matter (NOM) fouling of nanofiltration membranes. Journal of membrane science, 132(2), 159-181.

Hu, M., Zhao, L., Yu, N., Tian, Z., Yin, Z., Yang, Z., ... & Graham, N. J. (2021). Application of ultra-low concentrations of moderately-hydrophobic chitosan for ultrafiltration membrane fouling mitigation. Journal of Membrane Science, 119540.

Huang, B., Gu, H., Xiao, K., Qu, F., Yu, H., & Wei, C. (2020). Fouling mechanisms analysis via combined fouling models for surface water ultrafiltration process. Membranes, 10(7), 149.

Huang, Y., Xiao, C., Huang, Q., Liu, H., & Zhao, J. (2020). Progress on polymeric hollow fiber membrane preparation technique from the perspective of green and sustainable development. Chemical Engineering Journal, 126295.

Huang, Z., Ong, S. L., & Ng, H. Y. (2011). Submerged anaerobic membrane bioreactor for low strength wastewater treatment: effect of HRT and SRT on treatment performance and membrane fouling. Water research, 45(2), 705 713.

Hwang, K.J., Hsueh, C.L. (2003). Dynamic analysis of cake properties in microfiltration of soft colloids. Journal of Membrane Science 214, 259–273.

Iorhemen, O. T., Hamza, R. A., Zaghloul, M. S., & Tay, J. H. (2019). Aerobic granular sludge membrane bioreactor (AGMBR): Extracellular polymeric substances (EPS) analysis. Water research, 156, 305-314.

Iorhemen, O. T., & Liu, Y. (2021). Effect of feeding strategy and organic loading rate on the formation and stability of aerobic granular sludge. Journal of Water Process Engineering, 39, 101709.

Iorhemen, O. T. (2019). Development of Aerobic Granular Sludge Membrane Bioreactor (AGMBR) to Mitigate Fouling.

Iorhemen, O. T., Hamza, R. A., Sheng, Z., & Tay, J. H. (2019). Submerged aerobic granular sludge membrane bioreactor (AGMBR): Organics and nutrients (nitrogen and phosphorus) removal. Bioresource Technology Reports, 6, 260-267.

Iorhemen, O. T., Hamza, R. A., & Tay, J. H. (2016). Membrane bioreactor (MBR) technology for wastewater treatment and reclamation: membrane fouling. Membranes, 6(2), 33.

Iorhemen, O. T., Hamza, R. A., & Tay, J. H. (2017). Membrane fouling control in membrane bioreactors (MBRs) using granular materials. Bioresource technology, 240, 9-24.

Janus, T., Paul, P., & Ulanicki, B. (2009). Modelling and simulation of short- and long-term membrane filtration experiments. Desalination and Water Treatment, 8(1-3), 37-47.

Jawor, A., & Hoek, E. M. (2010). Removing cadmium ions from water via nanoparticle enhanced ultrafiltration. Environmental science & technology, 44(7), 2570-2576.

Jiang , HL.; Tay, JH.; Liu, Y.; Tay, STL. (2003) Ca2 + augmentation for enhancement of aerobically grown microbial granules in sludge blanket reactors. Biotechnol Lett, 25, 95.

Jiang, Z., Karan, S., & Livingston, A. G. (2019). Membrane Fouling: Does Microscale Roughness Matter?. Industrial & Engineering Chemistry Research, 59(12),5424-5431.

Jin, X., Jawor, A., Kim, S., & Hoek, E. M. (2009). Effects of feed water temperature on separation performance and organic fouling of brackish water RO membranes. Desalination, 239(1-3), 346-359.

Jin, X., Huang, X., & Hoek, E. M. (2009). Role of specific ion interactions in seawater RO membrane fouling by alginic acid. Environmental science & technology, 43(10), 3580 3587.

Juang, Y. C., Su, A., Fang, L. H., Lee, D. J., & Lai, J. Y. (2011). Fouling with aerobic granule membrane bioreactor. Water Science and Technology, 64(9), 1870 1875.

Kehrein, P., van Loosdrecht, M., Osseweijer, P., Dewulf, J., Garfi, M., & Duque, J. A. P. (2020). A critical review of resource recovery from municipal wastewater treatment plants market supply potentials, technologies and   bottlenecks. Environmental Science: Water Research & Technology.

Kennedy, M., Zhizhong, L., Febrina, E., van Hoof, S., Shippers, J. (2003).Effects of coagulation on filtration mechanisms in dead-end ultrafiltration. Water Science and Technology: Water Supply, 3(5-6), 109-116.

Kim, N. K., Mao, N., Lin, R., Bhattacharyya, D., van Loosdrecht, M. C., & Lin, Y. (2020). Flame retardant property of flax fabrics coated by extracellular   polymeric substances recovered from both activated sludge and aerobic granular sludge. Water research, 170, 115-344.

Kjelleberg, S., & Hermansson, M. (1984). Starvation-induced effects on bacterial surface characteristics. Applied and Environmental Microbiology, 48(3), 497-503.

Kos, B. V. Z. E., Šušković, J., Vuković, S., Šimpraga, M., Frece, J., & Matošić, S. (2003). Adhesion and aggregation ability of probiotic strain Lactobacillus acidophilus M92. Journal of applied microbiology, 94(6), 981-987.

Fujimori, K. (1959). The infrared spectra of Alkane-1-sulfonates. Bulletin of the Chemical Society of Japan, 32(8), 850-852.

Kwon, B., Lee, S., Cho, J., Ahn, H., Lee, D., Shin, H.S. (2005). Biodegradability, DBP formation, and membrane fouling potential of natural organic matter: Characterization and controllability. Environmental science & technology, 39(3), 732-739.

Lares, M., Ncibi, M.C., Sillanpaa, M., Sillanpaa, M. (2018). Occurrence, identification and removal of microplastic particles and fibers in conventional activated sludge process and advanced MBR technology. Water Res. 133, 236–246.

Lashkarizadeh, M., Munz, G., & Oleszkiewicz, J. A. (2016). Impacts of variable pH on stability and nutrient removal efficiency of aerobic granular sludge. Water Science and Technology, 73(1), 60-68.

Lay, H. T., Yeow, R. J. E., Ma, Y., Zydney, A. L., Wang, R., & Chew, J. W. (2021). Internal membrane fouling by proteins during microfiltration. Journal of Membrane Science, 637, 119589.

Lay, W.C.L., Liu, Y., Fane, A.G. (2010). Impacts of salinity on the performance of high retention membrane bioreactors for water reclamation: a review. Water Research 44, 21 40.

Le-Clech, P. (2010). Membrane bioreactors and their uses in wastewater treatments. Applied microbiology and biotechnology, 88(6), 1253-1260.

Lee, E. K., Chen, V., & Fane, A. G. (2008). Natural organic matter (NOM) fouling in low pressure membrane filtration—effect of membranes and operation modes. Desalination, 218(1-3), 257-270.

Lettmann, C., Möckel, D., & Staude, E. (1999). Permeation and tangential flow streaming potential measurements for electrokinetic characterization of track etched microfiltration membranes. Journal of membrane science, 159(1-2), 243-251.

Li, J., Yang, F., Liu, Y., Song, H., Li, D., Cheng, F. (2012). Microbial community and biomass characteristics associated severe membrane fouling during start-up of a hybrid anoxic–oxic membrane bioreactor. Bioresource technology, 103(1),43-47.

Li, X. F., Li, Y. J., Liu, H., Hua, Z. Z., Du, G. C., & Chen, J. (2008). Correlation between extracellular polymeric substances and aerobic biogranulation in membrane bioreactor. Separation and Purification Technology, 59(1), 26-33.

Liébana, R., Modin, O., Persson, F., & Wilén, B. M. (2018). Integration of aerobic granular sludge and membrane bioreactors for wastewater treatment. Critical reviews in biotechnology, 38(6), 801-816.

Lin, Y. M., Sharma, P. K., & Van Loosdrecht, M. C. M. (2013). The chemical andmechanical differences between alginate-like exopolysaccharides isolated from aerobic flocculent sludge and aerobic granular sludge. Water research, 47(1), 57-65.

Liu, L., Wang, Z., Yao, J., Sun, X., & Cai, W. (2005). Investigation on the properties and kinetics of glucose-fed aerobic granular sludge. Enzyme and Microbial Technology, 36(2-3), 307-313.

Liu, S. H., Yang, H., Ji, S. F., Gao, C. M., Fang, H., Xing, Y. Q., ... & Jia, L. (2019). Fabricating PES/SPSF membrane via reverse thermally induced phase separation (RTIPS) process to enhance permeability and hydrophilicity. RSC advances, 9(46), 26807-26816.

Liu, T., Chen, Z. L., Yu, W. Z., & You, S. J. (2011). Characterization of organic membrane foulants in a submerged membrane bioreactor with pre-ozonation using three dimensional excitation–emission matrix fluorescence spectroscopy. Water research, 45(5), 2111-2121.

Liu, X. Y., Chen, W., & Yu, H. Q. (2020). Probing protein-induced membrane fouling with in situ attenuated total reflectance fourier transform infrared spectroscopy and multivariate curve resolution-alternating least squares. Water Research, 183, 116052.

Liu, Y., Yang, S. F., Liu, Q. S., & Tay, J. H. (2003). The role of cell hydrophobicity in the formation of aerobic granules. Current microbiology, 46(4), 0270-0274.

Liu, Y., & Liu, Q. S. (2006). Causes and control of filamentous growth in aerobic granular sludge sequencing batch reactors. Biotechnology Advances, 24(1), 115-127.

Liu, Y. Q., & Tay, J. H. (2015). Fast formation of aerobic granules by combining strong hydraulic selection pressure with overstressed organic loading rate. Water research, 80, 256-266.

Liu, Y., & Tay, J. H. (2002). The essential role of hydrodynamic shear force in the formation of biofilm and granular sludge. Water Research, 36, 1653–1665.

Liu, Y., Yang, S. F., Tay, J. H., Liu, Q. S., Qin, L., & Li, Y. (2004). Cell hydrophobicity is a triggering force of biogranulation. Enzyme and Microbial Technology, 34(5), 371-379.

Liu, Y.; Lin, YM.; Yang, SF.; Tay, JH. (2003) A balanced model for biofilms developed at different growth and detachment forces. Process Biochem, 38, 1761.

Liu, Y. Q., & Tay, J. H. (2007). Characteristics and stability of aerobic granules cultivated with different starvation time. Applied microbiology and biotechnology, 75(1), 205-210.

Long, B., Yang, C. Z., Pu, W. H., Yang, J. K., Liu, F. B., Zhang, L., ... & Cheng, K. (2015). Tolerance to organic loading rate by aerobic granular sludge in a cyclic aerobic granular reactor. Bioresource technology, 182, 314-322.

Luján-Facundo, M. J., Mendoza-Roca, J. A., Cuartas-Uribe, B., & Álvarez-Blanco, S. (2015). Evaluation of cleaning efficiency of ultrafiltration membranes fouled by BSA using FTIR–ATR as a tool. Journal of food Engineering, 163, 1-8.

Luo, J., Hao, T., Wei, L., Mackey, H. R., Lin, Z., & Chen, G. H. (2014). Impact of influent COD/N ratio on disintegration of aerobic granular sludge. Water research, 62, 127-135.

Maltos, R. A., Holloway, R. W., & Cath, T. Y. (2020). Enhancement of activated sludge wastewater treatment with hydraulic selection. Separation and Purification Technology, 250, 117214.

Mänttäri, M., & Nyström, M. (2000). Critical flux in NF of high molar mass polysaccharides and effluents from the paper industry. Journal of membrane science, 170(2), 257-273.

McMurry, L.M., Oethinger, M., Levy, S.B. (1998). Triclosan targets lipid synthesis. Nature, 394 (6693), 531–532.

McSwain, B. S., Irvine, R. L., Hausner, M., & Wilderer, P. (2005). Composition and distribution of extracellular polymeric substances in aerobic flocs and granular sludge. Applied and environmental microbiology, 71(2), 1051-1057.

Melin, T., Jefferson, B., Bixio, D., Thoeye, C., De Wilde, W., De Koning, J., van der Graaf, J., Wintgens, T. (2006). Membrane bioreactor technology for wastewater treatment and reuse. Desalination 187 (1–3), 271–282.

Meng, F., Shi, B., Yang, F., & Zhang, H. (2007). Effect of hydraulic retention time on membrane fouling and biomass characteristics in submerged membrane bioreactors. Bioprocess and Biosystems Engineering, 30(5), 359-367.

Meng, F., Chae, S. R., Drews, A., Kraume, M., Shin, H. S., & Yang, F. (2009). Recent advances in membrane bioreactors (MBRs): membrane fouling and   membrane material. Water research, 43(6), 1489-1512.

Meng, F., Zhang, S., Oh, Y., Zhou, Z., Shin, H. S., & Chae, S. R. (2017). Fouling in membrane bioreactors: an updated review. Water research, 114, 151-180.

Meng, F., Liu, D., Pan, Y., Xi, L., Yang, D., and Huang, W. (2019). Enhanced amount and quality of alginate-like exopolysaccharides in aerobic granular sludge for the treatment of salty wastewater. BioRes. 14(1), 139-165.

Miller, D. J., Kasemset, S., Paul, D. R., & Freeman, B. D. (2014). Comparison of membrane fouling at constant flux and constant transmembrane pressure conditions. Journal of Membrane Science, 454, 505-515.

Modena, M. M., Rühle, B., Burg, T. P., & Wuttke, S. (2019). Nanoparticle characterization: what to measure?. Advanced Materials, 31(32), 1901556.

Mohammad, A. W., Teow, Y. H., Chong, W. C., & Ho, K. C. (2019). Hybrid Processes: Membrane Bioreactor. In Membrane Separation Principles and Applications (pp. 401-470). Elsevier.

Motlagh, A. M., Bhattacharjee, A. S., & Goel, R. (2015). Microbiological study of bacteriophage induction in the presence of chemical stress factors in enhanced biological phosphorus removal (EBPR). Water research, 81, 1-14.

Nancharaiah, Y. V., & Sarvajith, M. (2019). Aerobic granular sludge process: a fast-growing biological treatment for sustainable wastewater treatment. Current Opinion in Environmental Science & Health, 12, 57-65.

Nguyen, T. T., Kook, S., Lee, C., Field, R. W., & Kim, I. S. (2019). Critical flux based membrane fouling control of forward osmosis: Behavior, sustainability, and reversibility. Journal of membrane science, 570, 380-393.

Niermans, R., Giesen, A., Van Loosdrecht, M. C. M., & de Bruin, B. (2014). Full scale experiences with aerobic granular biomass technology for treatment of urban and industrial wastewater. In Proceedings of the Water Environment Federation, WEFTEC 014 (pp. 2347-2357).

Oh, J. H. (2007). Fundamental and application of aerobic granulation technology for wastewater treatment.

Pagotto Jr, R., Rossetto, R., Gasperi, R. L. P., Andrade, J. P., Trovati, J., Vallero, M.V. G., ... & Arntsen, B. (2014). SANASA Capivari II–the first full-scale municipal membrane bioreactor in Latin America. Water science and technology, 70(2), 272-278.

Park, H.D., Chang, I.S., Lee, K.J., 2015. Principles of Membrane Bioreactors for wastewater treatment. CRC Press.

Pearce, G., Introduction to membranes: Membrane selection. Filtration & Separation, 2007. 44(3): p. 35-37.

Pellegrin, M.-L., Neethling, J., Menniti, A., Sandino, J., Stensel, D. (2015). Application of Membrane Bioreactor Processes for Achieving Low Effluent Nutrient Concentrations. Water Environment Research Foundation; IWA Publishing.

Peng, W., Escobar, I. C., & White, D. B. (2004). Effects of water chemistries and properties of membrane on the performance and fouling—a model development study. Journal of membrane science, 238(1-2), 33-46.

Pronk, M., Abbas, B., Al-Zuhairy, S. H. K., Kraan, R., Kleerebezem, R., & Van Loosdrecht, M. C. M. (2015). Effect and behaviour of different substrates in relation to the formation of aerobic granular sludge. Applied microbiology and biotechnology, 99(12), 5257-5268.

Qin L, Tay JH, Liu Y. (2004) Selection pressure is a driving force of aerobic granulation in sequencing batch reactors. Process Biochem , 39, 579.

Rahimpour, A., Madaeni, S. S., & Mansourpanah, Y. (2010). Nano-porous polyethersulfone PES) membranes modified by acrylic acid (AA) and 2 hydroxyethylmethacrylate (HEMA) as additives in the gelation media. Journal of Membrane Science, 364(1-2), 380-388.

Rahman, M. M., Al-Sulaimi, S., & Farooque, A. M. (2018). Characterization of new and fouled SWRO membranes by ATR/FTIR spectroscopy. Applied Water Science, 8(6), 1-11.

Ranjan, R. (2021). Restoring natural wetlands through financial incentives based adoption of constructed wetlands on agricultural farms. Journal of Cleaner Production, 317, 128346.

Rehman, W. U., Muhammad, A., Younas, M., Wu, C., Hu, Y., & Li, J. (2019). Effect of membrane wetting on the performance of PVDF and PTFE membranes in the concentration of pomegranate juice through osmotic distillation. Journal of Membrane Science, 584, 66-78.

Rosenberg, M., Gutnick, D., & Rosenberg, E. (1980). Adherence of bacteria to hydrocarbons: a simple method for measuring cell-surface hydrophobicity. FEMS microbiology letters, 9(1), 29-33.

Rosenberger, S., Evenblij, H., te Poele, S., Wintgens, T., Laabs, C., 2005. The importance of liquid phase analyses to understand fouling in membrane assisted activated sludge processes—six case studies of different European research groups. Journal of Membrane Science, 263(1-2), 113-126.

Salgın, S., Takaç, S., & Özdamar, T. H. (2006). Adsorption of bovine serum albumin on polyether sulfone ultrafiltration membranes: Determination of interfacial interaction energy and effective diffusion coefficient. Journal of membrane   science, 278(1-2), 251-260.

Sarma, S. J., Tay, J. H., & Chu, A. (2017). Finding knowledge gaps in aerobic granulation technology. Trends in biotechnology, 35(1), 66-78.

Sheikholeslami, R., 2000. Calcium sulfate fouling – precipitation or particulate: a proposed composite model. Heat Transfer Engineering, 21(3), 24-33.

Shen, Y., Xiao, K., Liang, P., Sun, J., Sai, S., Huang, X., 2012. Characterization of soluble microbial products in 10 large-scale membrane bioreactors for municipal wastewater treatment in China. J. Membr. Sci. 415–416, 336–345.

Show, K. Y., Lee, D. J., & Tay, J. H. (2012). Aerobic granulation: advances and challenges. Applied Biochemistry and Biotechnology, 167(6), 1622-1640.

Solon, K., Volcke, E. I., Spérandio, M., & van Loosdrecht, M. C. (2019). Resource recovery and wastewater treatment modelling. Environmental Science: Water Research & Technology, 5(4), 631-642.

Stes, H., Aerts, S., Caluwé, M., Dobbeleers, T., Wuyts, S., Kiekens, F., ... & Dries, J. (2018). Formation of aerobic granular sludge and the influence of the pH on sludge characteristics in a SBR fed with brewery/bottling plant wastewater. Water Science and Technology, 77(9), 2253-2264.

Sun, J., Xiao, K., Mo, Y., Liang, P., Shen, Y., Zhu, N., Huang, X., 2014a. Seasonal characteristics of supernatant organics and its effect on membrane fouling in a full-scale membrane bioreactor. J. Membr. Sci. 453, 168–174.

Sun, C., Zhang, N., Li, F., Ke, G., Song, L., Liu, X., & Liang, S. (2018). Quantitative analysis of membrane fouling mechanisms involved in microfiltration of humic acid protein mixtures at different solution conditions. Water, 10(10), 1306.

Talvitie, J., Mikola, A., Koistinen, A., Setala, O., 2017. Solutions to microplastic pollution removal of microplastics from wastewater effluent with advanced wastewater treatment technologies. Water Res. 123, 401–407.

Tang, C.Y., Y.-N. Kwon, and J.O. Leckie, Characterization of humic acid fouled reverse osmosis and nanofiltration membranes by transmission electron microscopy and streaming potential measurements. Environmental science & technology, 2007. 41(3): p. 942-949.

Tang, S., Wang, Z., Wu, Z., Zhou, Q., 2010. Role of dissolved organic matters (DOM) in membrane fouling of membrane bioreactors for municipal wastewater treatment. Journal of Hazardous Materials 178, 377–384.

Tay JH, Ivanov V, Pan S, Tay STL. (2002d) Specific layers in aerobically grown microbial granules. Lett Appl

Tay STL, Ivanov V, Yi S, Zhuang WQ, Tay JH. (2002e) Presence of anaerobic Bacteroides in aerobically grown microbial granules. Microb Ecol, 44, 278.

Tay, J. H., Liu, Q. S., & Liu, Y. (2001). The effects of shear force on the formation, structure and metabolism of aerobic granules. Applied microbiology and biotechnology, 57(1), 227-233.

Tay, J. H., Liu, Q. S., & Liu, Y. (2002). Characteristics of aerobic granules grown on glucose and acetate in sequential aerobic sludge blanket reactors. Environmental technology, 23(8), 931-936.

Tay, J. H., Pan, S., He, Y., & Tay, S. T. L. (2004). Effect of organic loading rate on aerobic granulation. I: Reactor performance. Journal of environmental engineering, 130(10), 1094-1101.

Tay, J. H., Tay, S. T. L., Show, K. Y., Liu, Y., & Ivanov, V. (2004). U.S. Patent No. 6,793,822. Washington, DC: U.S. Patent and Trademark Office.

Tay, J.-H., et al., Aerobic Granulation Technology, in Advanced Biological Treatment Processes, L.K. Wang, N.K. Shammas, and Y.-T. Hung, Editors. 2009, Humana Press: Totowa, NJ. p. 109-128.

Tay, J.H., Q.S. Liu, and Y. Liu, The role of cellular polysaccharides in the formation and stability of aerobic granules. Lett Appl Microbiol, 2001. 33(3): p. 222-6. Technol. 129, 526–531.

UNESCO, 2017, World Water Development Report, Wastewater: The untapped resource, https://reliefweb.int/report/world/2017-un-world-water development-report-wastewater untapped-resource, Accessed March 10, 2020.

USEPA. (2010). NPDES Permit Writers' Manual,   https://www.epa.gov/sites/default/files/2015 09/documents/pwm_chapt_05.pdf, Accessed September, 2015

Van Der Roest, H., Van Loosdrecht, M. C. M., Langkamp, E. J., & Uijterlinde, C. (2015). Recovery and reuse of alginate from granular Nereda sludge. Water 21, 17(2), 48.

Vatanpour, V., M. Esmaeili, and M.H.D.A. Farahani, Fouling reduction and retention increment of polyethersulfone nanofiltration membranes embedded by amine functionalized multi-walled carbon nanotubes. Journal of Membrane Science,   2014. 466: p. 70-81.

Wang, L., Liang, W., Chen, W., Zhang, W., Mo, J., Liang, K., ... & Jiang, F. (2018). Integrated aerobic granular sludge and membrane process for enabling municipal wastewater treatment and reuse water production. ChemicalEngineering Journal, 337, 300-311.

Wang, Z., Liu, L., Yao, J., & Cai, W. (2006). Effects of extracellular polymeric substances on aerobic granulation in sequencing batch reactors. Chemosphere, 63(10), 1728-1735.

Wang, Z., Wu, Z., & Tang, S. (2009). Extracellular polymeric substances (EPS) properties and their effects on membrane fouling in a submerged membrane bioreactor. Water research, 43(9), 2504-2512.

Wei, D., Qiao, Z., Zhang, Y., Hao, L., Si, W., Du, B., & Wei, Q. (2013). Effect of COD/N ratio on cultivation of aerobic granular sludge in a pilot-scale sequencing batch reactor. Applied microbiology and biotechnology, 97(4), 1745-1753.

Wickramasinghe, S. R., Bower, S. E., Chen, Z., Mukherjee, A., & Husson, S. M.(2009). Relating the pore size distribution of ultrafiltration membranes to dextran rejection. Journal of Membrane Science, 340(1-2), 1-8.

Wilén, B. M., Liébana, R., Persson, F., Modin, O., & Hermansson, M. (2018). The mechanisms of granulation of activated sludge in wastewater treatment, its optimization, and impact on effluent quality. Applied microbiology and biotechnology, 102(12), 5005 5020.

Woo, S. H., Park, J., & Min, B. R. (2015). Relationship between permeate flux and surface roughness of membranes with similar water contact angle values. Separation and purification technology, 146, 187-191.

Wu, L., Wei, Q., Zhang, Y., Fan, Y., Li, M., Rong, L., ... & Zou, X. (2021). Effects of antibiotics on enhanced biological phosphorus removal and its mechanisms. Science of The Total Environment, 145571.

Xagoraraki, I., Yin, Z., Svambayev, Z. (2014). Fate of viruses in water systems. J. Environ.Eng. 140 (7).

Xin, X., & Qin, J. (2019). Rapid start-up of partial nitritation in aerobic granular sludge bioreactor and the analysis of bacterial community dynamics. Bioprocess and biosystems engineering, 42(12), 1973-1981.

Yi, K., Wang, D., Li, X., Chen, H., Sun, J., An, H., ... & Zeng, G. (2017). Effect of ciprofloxacin on biological nitrogen and phosphorus removal from wastewater. Science of the Total Environment, 605, 368-375.

Yigit, N. O., Harman, I., Civelekoglu, G., Koseoglu, H., Cicek, N., & Kitis, M. (2008). Membrane fouling in a pilot-scale submerged membrane bioreactor operated under various conditions. Desalination, 231(1-3), 124-132.

Yuan, Q., Gong, H., Xi, H., Xu, H., Jin, Z., Ali, N., & Wang, K. (2019). Strategies to improve aerobic granular sludge stability and nitrogen removal based on feeding mode and substrate. Journal of Environmental Sciences, 84, 144-154.

Zhang, B., Huang, D., Shen, Y., Yin, W., Gao, X., & Shi, W. (2020). Treatment of
        municipal wastewater with aerobic granular sludge membrane bioreactor   (AGMBR):
performance and membrane fouling. Journal of Cleaner   Production, 273, 123124.

Zhang, W., & Jiang, F. (2019). Membrane fouling in aerobic granular sludge (AGS)
        membrane bioreactor (MBR): Effect of AGS size. Water research, 157, 445   453.

Zhang, W., Liang, W., Zhang, Z., & Hao, T. (2021). Aerobic granular sludge (AGS)
        scouring to mitigate membrane fouling: Performance, hydrodynamic mechanism and
        contribution quantification model. Water Research, 188, 116-518.

Zhao, J., Wang, Z., Ghosh, S., & Xing, B. (2014). Phenanthrene binding by humicacid–protein
        complexes as studied by passive dosing technique. Environmental pollution, 184, 145
        153.

Zhou, J. H., Zhang, Z. M., Zhao, H., Yu, H. T., Alvarez, P. J., Xu, X. Y., & Zhu, L. (2016).
        Optimizing granules size distribution for aerobic granular sludge stability: effect of a
        novel funnel-shaped internals on hydraulic shear stress. Bioresource technology, 216,
        562-570.

Zhu, L., Dai, X., Yu, Y. W., Qi, H. Y., & Xu, X. Y. (2012). Role and significance of
        extracellular polymeric substances on the property of aerobic granule. Bioresource
        technology, 107, 46-54.

Zhu, T., Xie, Y. H., Jiang, J., Wang, Y. T., Zhang, H. J., & Nozaki, T. (2009). Comparative
        study of polyvinylidene fluoride and PES flat membranes in submerged MBRs to treat
        domestic wastewater. Water Science and Technology, 59(3), 399-405.

Zuber, M., Zia, K. M., & Barikani, M. (2013). Chitin and chitosan based blends, composites and
        nanocomposites. In Advances in natural polymers (pp. 55-119). Springer, Berlin,
        Heidelberg.